

Article

Mathematical Approach for Mechanical Behaviour Analysis of FGM Plates on Elastic Foundation

Fatima Zohra Zaoui ¹, Djamel Ouinas ¹, Belkacem Achour ^{2,*}, Mabrouk Touahmia ², Mustapha Boukendakdji ², Enamur R. Latifee ², Ahmed A. Alawi Al-Naghi ²  and Jaime Aurelio Viña Olay ³ 

¹ Laboratory of Science and Technology Environment and Valorization, Faculty of Sciences and Technology, Ibn Badis University, Mostaganem 27000, Algeria

² Civil Engineering Department, University of Ha'il, Ha'il 55476, Saudi Arabia

³ Department of Materials Science and Metallurgical Engineering, University of Oviedo, Viesques Campus, 33203 Gijón, Spain

* Correspondence: b.achour@uoh.edu.sa

Abstract: This paper presents the flexural analysis of functionally graded plates resting on elastic foundations using new two-dimensional (2D) and quasi-three-dimensional (quasi-3D) higher order shear deformation theories. The main interesting feature of this theory is that it proposes a new displacement field with undetermined integral variables which involves only five unknown functions, unlike other shear and normal deformation theories, hence making it easier to use. A parabolic transverse shear deformation shape function satisfying the zero shear stress conditions on the plate outer surfaces is considered. The elastic foundation follows the Pasternak mathematical model. The material properties change continuously across the thickness of the FG plate using different distributions: power law, exponential, and Mori–Tanaka models. The governing equations of FG plates subjected to sinusoidal and uniformly distributed loads are established through the principle of virtual works and then solved via Navier's procedure. In this work, a detailed discussion on the influence of material composition, geometric parameters, stretching effect, and foundation parameters on the deflection, axial displacements, and stresses is given, and the obtained results are compared with those published in previous works to demonstrate the accuracy and the simplicity of the present formulations. The different obtained results were found to be in good agreement with the available solutions of other higher-order theories. The proposed model is able to represent the cross section warping in the deformed shape and to demonstrate the validity and efficiency of the approach, the findings reported herein prove that this theory is capable of predicting displacements and stresses more accurately than other theories, as its results are closer when compared to numerical methods reported in other literatures.

Keywords: bending; stress; functionally graded plate; shear deformation theory; stretching effect; Winkler–Pasternak parameters

MSC: 74E30; 74K20



Citation: Zaoui, F.Z.; Ouinas, D.; Achour, B.; Touahmia, M.; Boukendakdji, M.; Latifee, E.R.; Al-Naghi, A.A.A.; Viña Olay, J.A. Mathematical Approach for Mechanical Behaviour Analysis of FGM Plates on Elastic Foundation. *Mathematics* **2022**, *10*, 4764. <https://doi.org/10.3390/math10244764>

Academic Editors: Carlos Llopis-Albert and Fernando Simoes

Received: 17 October 2022

Accepted: 6 December 2022

Published: 15 December 2022

Publisher's Note: MDPI stays neutral with regard to jurisdictional claims in published maps and institutional affiliations.



Copyright: © 2022 by the authors. Licensee MDPI, Basel, Switzerland. This article is an open access article distributed under the terms and conditions of the Creative Commons Attribution (CC BY) license (<https://creativecommons.org/licenses/by/4.0/>).

1. Introduction

Functionally graded materials (FGMs) are a new type of advanced composite materials made up of a combination of ceramics and metals that is designed to endure high thermal environment and to provide stiffness to the host structure [1]. Their mechanical properties are assumed to change following a smooth and continuous distribution from the lower to the upper surface of the structure and thus eliminate stress concentration found in laminate composites and maintain structural integrity at a desirable level [2]. Due to this feature, FGMs have been explored in many engineering applications, such as aerospace, aircraft, automobile, and defence industries and most recently, electronic and biomedical applications [3,4].

In recent years, due to widespread applications of FGMs in various engineering fields, many theories have been developed in order to analyse bending, buckling and dynamic behaviours of different FG structures [5–9]. The use of plates resting on elastic foundations is very popular in structural engineering, such as reinforced concrete pavements, airport runways, storage tanks foundations, swimming pools, retaining walls, and concrete footings [10–13]. The most famous model of elastic foundations is known as the Winkler–Pasternak model. This contains, of course, two parameters—Winkler’s transverse stiffness coefficient and Pasternak’s shear stiffness coefficient. The first parameter of the Pasternak model represents the modelling of the elastic medium as a series of closely spaced, mutually independent vertical linear elastic springs, while the second parameter represents the transverse shear stress due to the interaction of the shear deformation of the surrounding elastic medium [14–18].

The bending problem of transverse load acting on an isotropic inhomogeneous rectangular plate using both two-dimensional (2D) trigonometric and three-dimensional (3D) elasticity solutions was analysed by Zenkour [19]. Additionally, the stress and displacement response of the FG plates resting on Pasternak elastic foundations have been analysed under uniform thermal and mechanical loading by Zenkour [20]. The effects of thickness stretching in functionally graded plates and shells were studied in a paper by Carrera et al. [21], in which variable plate/shell models are implemented according to Carrera’s unified formulation. Quasi-3D sinusoidal and hyperbolic shear deformation theories to study the static and free vibration responses of FG plates were proposed by Neves et al. [22,23]. Based on a simple refined higher-order shear deformation theory with two variables, Thai et al. [24] examined the bending, buckling and free vibration of thick FG plates resting on elastic foundation. The buckling response of a composite laminated material square plate having an elliptical notch was studied by Ouinas and Achour [25] using the finite element method. Mantari and Soares [26] developed an analytical solution to the static analysis of functionally graded plates by using a new trigonometric higher-order theory in which the stretching effect is included. A 3D elasticity solution for bending thick FG plates was proposed by Zhang et al. [27] using a hybrid semi-analytical approach—the state-space-based differential quadrature method. The influence of temperature and moisture on the bending behaviour of FG plates resting on elastic foundations using refined shear and normal deformations plate theory were investigated by Al Khateeb and Zenkour [28]. Thai and Choi [29] used a zeroth-order shear deformation theory for bending and vibration analyses of functionally graded plates resting on elastic foundation. A refined higher-order shear and normal deformation theory for E-, P-, and S-FGM plates on Pasternak elastic foundation was presented by Lee et al. [30]. Akavci and Tanrikulu [31] presented 2D and quasi-3D shear deformation theories for bending and free vibration analysis of single-layer FG plates using a new hyperbolic shape function. Mantari and Granados [32] developed an original first shear deformation theory for bending and free vibration analysis of functionally graded plates resting on elastic foundation. Houari et al. [33] developed a new simple and accurate three-unknowns sinusoidal shear deformation theory for the bending and vibration analysis of FG plates. Recently, a bending analysis of different material distributions of functionally graded beam was established by Aldousari [34], in which two symmetric and anti-symmetric functions were developed and their effects on the static deflection and bending stresses were compared with classical power law distribution. A non-polynomial four-refined-shear deformation theory for free vibration analysis of FG plates on elastic foundation was performed by Meftah et al. [35]. Zaoui et al. [36] and Guerroudj et al. [37] presented hybrid quasi-3D shear deformation theories to study the free vibration of functionally graded plates. A new simple shear deformation theory with three unknown was developed by Amar et al. [38] for static analysis of FG plates on elastic foundation. Younsi et al. [39] developed a non-polynomial 2D and quasi-3D theory to investigate static and dynamic responses of FG plates. Belkhodja et al. [40] investigated the flexion, free vibrations and buckling of FGMs plate with simply supported edges using a new exponential-trigonometric shear function. Thermal vibration of functionally

graded graphene platelets reinforced composite (FG-GPLRC) annular plate resting on an elastic foundation under the mechanical load framework of higher order shear deformation (HSDT) was analysed by Wang et al. [41]. Many researchers [42–45] have studied the flows of MHD hybrid nanofluid, while Qureshi et al. [46] have specially investigated the dispersion of polymer matrix/CNT nanocomposite material through permeable surfaces subjected to the magnetized hybrid nanofluids. The deduced mathematical model for nanocomposites based on PDEs is beneficial for nanotechnology. The analytical solutions for the temperature and velocity fields are obtained using the Laplace transform. The discrete fractional proportional operator, the Caputo and Caputo–Fabrizio fractional operators have been studied in references [47,48]. Vieru et al. [49] used the fractional time derivative of Caputo–Fabrizio to develop a new mathematical model. The latter is based on a fractional constitutive equation of the clean heat flux to describe the memory effects. Saffari et al. [50] used a size-dependent non-local strain gradient theory to analyse free and forced vibration responses of fluid-conveying viscoelastic nanotubes sitting on nonlinear Visco–Pasternak foundations under magnetic fields. Alazwari et al. [51] used the Visco–Winkler–Pasternak elastic foundation model in conjunction with a quasi-3D refined theory for the first time to study the vibration response of FG plates.

The objective of this work is to study the static behaviour of FG plates simply supported and resting on elastic foundations of the Winkler–Pasternak type by applying modified 2D and quasi-3D shear strain theories developed by Zaoui et al. [52], for which only the problem of free vibration of FGM plates resting on elastic supports was assessed. The most interesting feature of these theories is that they have a new displacement field that contains fewer unknowns compared to other theories such as Neves et al. [22,23]. Indeterminate integrals have been used in the proposed field of displacements in which the transverse shear and thickness stretching effects are considered in quasi-3D theory while ignored in the 2D model. Moreover, these theories account for a parabolic variation of transverse shear stresses across the thickness to satisfy shear stress free boundary conditions without including shear correction factor. The principle of virtual work is applied to establish the fundamental governing equations of FG plates subjected to sinusoidal and uniformly distributed loads. Closed-form solutions of deflections for simply supported plates are derived via Navier’s method, and the found results are compared to those published in the literature to demonstrate accuracy and simplicity of the proposed theories. The effects of power law index, slenderness ratio, side-to-thickness ratio, normal strain, Winkler–Pasternak parameters, and different rules of mixture on the bending response of FG plates have been carried out. The findings presented here demonstrate that the suggested model can accurately describe the cross section warping in the deformed shape and that it can estimate displacements and stresses of FG plates more precisely than other shear deformation theories.

2. Mathematical Formulation

2.1. Material Properties

In this work, a functionally graded rectangular plate, having uniform thickness h , length a , width b , is considered as seen in Figure 1. The material properties of FGM are assumed to vary gradually through the thickness according to the following rules of mixture.

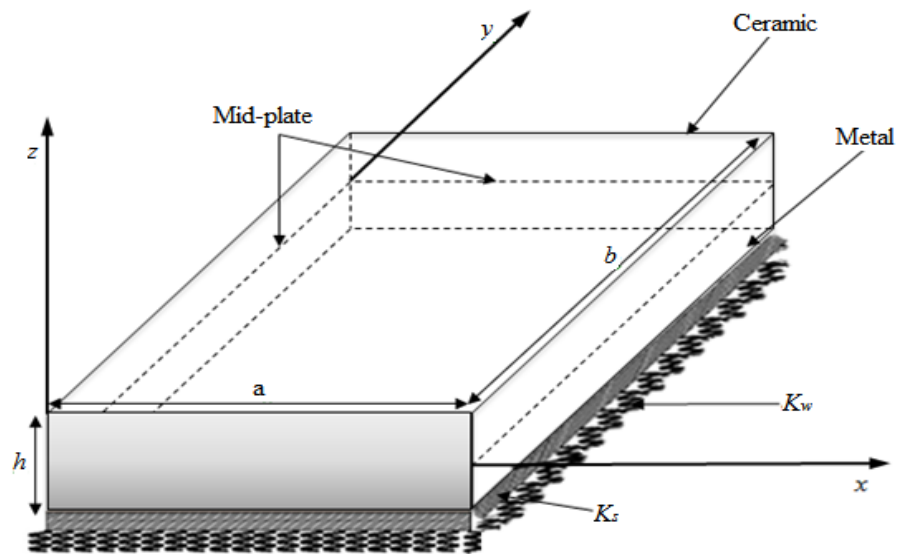


Figure 1. Geometry and coordinates of the considered FGM plate on elastic foundation.

2.1.1. The Power Law (P-FGM) Variation

The volume fraction of the P-FGM plate is supposed to change continuously across the thickness of the plate according to the power law variation [53], as given in Equation (1):

$$P(z) = P_m + (P_c - P_m) \left(\frac{1}{2} + \frac{z}{h} \right)^k \tag{1}$$

2.1.2. The Exponential (E-FGM) Variation

The volume fraction of the E-FGM plate is considered to vary continuously across the thickness direction of the plate according to the exponential distribution [30,54] as follows:

$$P(z) = P_m e^{p(z+h/2)}, \quad p = \frac{1}{h} \ln \left(\frac{P_c}{P_m} \right) \tag{2}$$

2.1.3. The Mori–Tanaka Homogenization Model

For the Mori–Tanaka scheme [29,39], the volume fraction of the FGM plate is defined in the equations below:

$$P(z) = P_m + (P_c - P_m) \frac{V_c}{1 + V_m \left(\frac{P_c}{P_m} - 1 \right)^{\frac{1+\nu}{3-3\nu}}}, \tag{3a}$$

$$V_c = \left(\frac{1}{2} + \frac{z}{h} \right)^k, \quad V_m + V_c = 1 \tag{3b}$$

where P represents the effective material property, such as Young’s modulus E . P_m , P_c , V_m and V_c denote material properties and the volume fraction of the upper (metal) and the lower (ceramic) faces of the plate, respectively. k is the power law index and P is the volume fraction exponent. Since the effects of Poisson’s ratio (ν) on the response of FG plates are very small, they are supposed to be constant for all FGM graded layers.

2.2. Kinematics

On the basis of higher-order shear deformation theories and considering the stretching effect [52,55], the supposed displacement field of the plate can be expressed as

$$\begin{aligned}
 u(x, y, z, t) &= u_0(x, y, t) - z \frac{\partial w_0}{\partial x} + k_1 f(z) \int \theta(x, y, t) dx \\
 v(x, y, z, t) &= v_0(x, y, t) - z \frac{\partial w_0}{\partial y} + k_2 f(z) \int \theta(x, y, t) dy \\
 w(x, y, z, t) &= w_0(x, y, t) + g(z) \phi_z(x, y, t)
 \end{aligned}
 \tag{4}$$

where u_0, v_0, w_0, θ and ϕ_z are the five unknown displacement functions of the middle surface of the plate. Note that the integrals do not have limits. The constants k_1 and k_2 depend on the geometry. $f(z)$ is the shape function which represents the variation of the transverse shear strains within the thickness. Note that $g(z) = 0$ for 2D analysis.

The shape function is chosen according to Zaoui et al. [9,52] as

$$f(z) = \frac{\pi h}{\pi^4 + h^4} e^{(hz/\pi)} \left(\pi^2 \sin\left(\frac{\pi z}{h}\right) + h^2 \cos\left(\frac{\pi z}{h}\right) \right) - \frac{\pi h^3}{\pi^4 + h^4}
 \tag{5a}$$

and

$$g(z) = \frac{df}{dz}
 \tag{5b}$$

The general strain–displacement relations can be defined from Equation (4) by the application of the linear small-strain elasticity theory as follows

$$\begin{Bmatrix} \varepsilon_x \\ \varepsilon_y \\ \gamma_{xy} \end{Bmatrix} = \begin{Bmatrix} \varepsilon_x^0 \\ \varepsilon_y^0 \\ \gamma_{xy}^0 \end{Bmatrix} + z \begin{Bmatrix} k_x^b \\ k_y^b \\ k_{xy}^b \end{Bmatrix} + f(z) \begin{Bmatrix} k_x^s \\ k_y^s \\ k_{xy}^s \end{Bmatrix}
 \tag{6a}$$

$$\begin{Bmatrix} \gamma_{yz} \\ \gamma_{xz} \end{Bmatrix} = g(z) \begin{Bmatrix} \gamma_{yz}^0 \\ \gamma_{xz}^0 \end{Bmatrix}, \varepsilon_z = g'(z) \varepsilon_z^0
 \tag{6b}$$

where

$$\begin{Bmatrix} \varepsilon_x^0 \\ \varepsilon_y^0 \\ \gamma_{xy}^0 \end{Bmatrix} = \begin{Bmatrix} \frac{\partial u_0}{\partial x} \\ \frac{\partial v_0}{\partial x} \\ \frac{\partial u_0}{\partial y} + \frac{\partial v_0}{\partial x} \end{Bmatrix}, \begin{Bmatrix} k_x^b \\ k_y^b \\ k_{xy}^b \end{Bmatrix} = \begin{Bmatrix} -\frac{\partial^2 w_0}{\partial x^2} \\ -\frac{\partial^2 w_0}{\partial y^2} \\ -2\frac{\partial^2 w_0}{\partial x \partial y} \end{Bmatrix}
 \tag{7a}$$

$$\begin{Bmatrix} k_x^s \\ k_y^s \\ k_{xy}^s \end{Bmatrix} = \begin{Bmatrix} k_1 \theta \\ k_2 \theta \\ k_1 \frac{\partial}{\partial y} \int \theta dx + k_2 \frac{\partial}{\partial x} \int \theta dy \end{Bmatrix},
 \tag{7b}$$

$$\begin{Bmatrix} \gamma_{yz}^0 \\ \gamma_{xz}^0 \end{Bmatrix} = \begin{Bmatrix} k_2 \int \theta dy + \frac{\partial \phi_z}{\partial y} \\ k_1 \int \theta dx + \frac{\partial \phi_z}{\partial x} \end{Bmatrix},
 \tag{7c}$$

$$\varepsilon_z^0 = \phi_z \text{ and } g'(z) = \frac{dg(z)}{dz}
 \tag{7d}$$

It can be seen from Equation (6) that the transverse shear strains (γ_{xz}, γ_{yz}) are equal to zero at the top ($z = h/2$) and bottom ($z = -h/2$) surfaces of the plate. A shear correction coefficient is, hence, not required.

The integrals employed in the above expressions are solved by a Navier’s type solution and can be described as

$$\frac{\partial}{\partial y} \int \theta dx = A' \frac{\partial^2 \theta}{\partial x \partial y}, \quad \frac{\partial}{\partial x} \int \theta dy = B' \frac{\partial^2 \theta}{\partial x \partial y} \tag{8a}$$

$$\int \theta dx = A' \frac{\partial \theta}{\partial x}, \quad \int \theta dy = B' \frac{\partial \theta}{\partial y} \tag{8b}$$

where the coefficients A' and B' —which are defined according to the type of solutions employed, k_1 and k_2 —are expressed as follows:

$$A' = -\frac{1}{\alpha^2}, \quad B' = -\frac{1}{\beta^2}, \quad k_1 = \alpha^2, \quad k_2 = \beta^2 \tag{9}$$

Note that α and β are defined in Equation (24).

The stress–strain relationships for FG plate according to three-dimensional (3D) elasticity can be written as

$$\begin{Bmatrix} \sigma_x \\ \sigma_y \\ \sigma_z \\ \tau_{yz} \\ \tau_{xz} \\ \tau_{xy} \end{Bmatrix} = \begin{bmatrix} Q_{11} & Q_{12} & Q_{13} & 0 & 0 & 0 \\ Q_{12} & Q_{22} & Q_{23} & 0 & 0 & 0 \\ Q_{13} & Q_{23} & Q_{33} & 0 & 0 & 0 \\ 0 & 0 & 0 & Q_{44} & 0 & 0 \\ 0 & 0 & 0 & 0 & Q_{55} & 0 \\ 0 & 0 & 0 & 0 & 0 & Q_{66} \end{bmatrix} \begin{Bmatrix} \varepsilon_x \\ \varepsilon_y \\ \varepsilon_z \\ \gamma_{yz} \\ \gamma_{xz} \\ \gamma_{xy} \end{Bmatrix} \tag{10}$$

The Q_{ij} expressions in terms of engineering constants depend on the normal strain ε_z .

- If the $\varepsilon_z \neq 0$ then Q_{ij} are

$$Q_{11} = Q_{22} = Q_{33} = \frac{(1 - \nu)E(z)}{(1 - 2\nu)(1 + \nu)} \tag{11a}$$

$$Q_{12} = Q_{13} = Q_{23} = \frac{\nu E(z)}{(1 - 2\nu)(1 + \nu)} \tag{11b}$$

$$Q_{44} = Q_{55} = Q_{66} = \frac{E(z)}{2(1 + \nu)} \tag{11c}$$

- If the $\varepsilon_z = 0$, then Q_{ij} are

$$Q_{11} = Q_{22} = \frac{E(z)}{(1 - \nu^2)} \tag{12a}$$

$$Q_{12} = \frac{\nu E(z)}{(1 - \nu^2)} \tag{12b}$$

$$Q_{44} = Q_{55} = Q_{66} = \frac{E(z)}{2(1 + \nu)} \tag{12c}$$

2.3. Equilibrium Equations and Stress Components

The equilibrium equations of functionally graded plate subjected to mechanical loadings can be derived by applying the principle of virtual works [56], which can be expressed in analytical form as

$$0 = \delta U + \delta V_p + \delta V_e \tag{13}$$

where δU is the virtual strain energy, δV_p is the virtual potential energy of applied distributed transverse loads, and δV_e is the virtual strain energy of the elastic foundation.

The virtual strain energy of the plate is defined by

$$\begin{aligned} \delta U &= \int_V [\sigma_x \delta \varepsilon_x + \sigma_y \delta \varepsilon_y + \sigma_z \delta \varepsilon_z + \tau_{xy} \delta \gamma_{xy} + \tau_{yz} \delta \gamma_{yz} + \tau_{xz} \delta \gamma_{xz}] dV \\ &= \int_A [N_x \delta \varepsilon_x^0 + N_y \delta \varepsilon_y^0 + N_z \delta \varepsilon_z^0 + N_{xy} \delta \gamma_{xy}^0 + M_x^b \delta k_x^b + M_y^b \delta k_y^b \\ &\quad + M_{xy}^b \delta k_{xy}^b + M_x^s \delta k_x^s + M_y^s \delta k_y^s + M_{xy}^s \delta k_{xy}^s + Q_{yz}^s \delta \gamma_{yz}^0 + Q_{xz}^s \delta \gamma_{xz}^0] dA \end{aligned} \tag{14}$$

where A is the top surface and the stress resultants N , M and Q are given by

$$(N_i, M_i^b, M_i^s) = \int_{-h/2}^{h/2} (1, z, f) \sigma_i dz, \quad (i = x, y, xy) \tag{15a}$$

$$N_z = \int_{-h/2}^{h/2} g'(z) \sigma_z dz \tag{15b}$$

$$(Q_{xz}^s, Q_{yz}^s) = \int_{-h/2}^{h/2} g(\tau_{xz}, \tau_{yz}) dz \tag{15c}$$

The virtual potential energy of the applied external loads to the plate can be expressed as

$$\delta V_p = - \int_A q \delta w_0 dA \tag{16}$$

where q is the external load applied to the plate.

The virtual strain energy of the foundation can be written as

$$\delta V_e = \int_A \left[K_w w_0 \delta w_0 + K_s \left(\frac{\partial w_0}{\partial x} \frac{\partial \delta w_0}{\partial x} + \frac{\partial w_0}{\partial y} \frac{\partial \delta w_0}{\partial y} \right) \right] dA \tag{17}$$

where K_w and K_s are the transverse and shear stiffness coefficients of the foundation, respectively.

The governing equations of equilibrium can be obtained by substituting Equations (14), (16) and (17) into Equation (13), integrating the displacement gradients by parts, and setting the coefficients δu_0 , δv_0 , δw_0 , $\delta \theta$ and $\delta \phi_z$ to zero separately, as follows:

$$\delta u_0 : \frac{\partial N_x}{\partial x} + \frac{\partial N_{xy}}{\partial y} = 0 \tag{18a}$$

$$\delta v_0 : \frac{\partial N_y}{\partial y} + \frac{\partial N_{xy}}{\partial x} = 0 \tag{18b}$$

$$\delta w_0 : \frac{\partial^2 M_x^b}{\partial x^2} + \frac{\partial^2 M_y^b}{\partial y^2} + 2 \frac{\partial^2 M_{xy}^b}{\partial x \partial y} - K_w w_0 + K_s \nabla^2 w_0 = -q \tag{18c}$$

$$\delta \theta : -k_1 M_x^s - k_2 M_y^s - (k_1 A' + k_2 B') \frac{\partial^2 M_{xy}^s}{\partial x \partial y} + k_1 A' \frac{\partial S_{xz}^s}{\partial x} + k_2 B' \frac{\partial S_{yz}^s}{\partial y} = 0 \tag{18d}$$

$$\delta\phi_z : \frac{\partial S_{xz}^s}{\partial x} + \frac{\partial S_{yz}^s}{\partial y} - N_z = 0 \tag{18e}$$

where $\nabla^2 = (\partial^2/\partial x^2) + (\partial^2/\partial y^2)$ is the Laplacian operator in a 2D Cartesian coordinate system.

The stresses and moment resultants which appeared in Equation (15) can be written in terms of generalized displacements $(u_0, v_0, w_0, \theta, \phi_z)$ as:

$$\begin{pmatrix} N_x \\ N_y \\ N_{xy} \\ M_x^b \\ M_y^b \\ M_{xy}^b \\ M_x^s \\ M_y^s \\ M_{xy}^s \\ N_z \end{pmatrix} = \begin{bmatrix} A_{11} & A_{12} & 0 & B_{11} & B_{12} & 0 & B_{11}^s & B_{12}^s & 0 & X_{13} \\ A_{12} & A_{22} & 0 & B_{12} & B_{22} & 0 & B_{12}^s & B_{22}^s & 0 & X_{23} \\ 0 & 0 & A_{66} & 0 & 0 & B_{66} & 0 & 0 & B_{66}^s & 0 \\ B_{11} & B_{12} & 0 & D_{11} & D_{12} & 0 & D_{11}^s & D_{12}^s & 0 & Y_{13} \\ B_{12} & B_{22} & 0 & D_{12} & D_{22} & 0 & D_{12}^s & D_{22}^s & 0 & Y_{23} \\ 0 & 0 & B_{66} & 0 & 0 & D_{11} & 0 & 0 & D_{66}^s & 0 \\ B_{11}^s & B_{12}^s & 0 & D_{11}^s & D_{12}^s & 0 & H_{11}^s & H_{12}^s & 0 & Y_{13}^s \\ B_{12}^s & B_{22}^s & 0 & D_{12}^s & D_{22}^s & 0 & H_{12}^s & H_{22}^s & 0 & Y_{23}^s \\ 0 & 0 & B_{66}^s & 0 & 0 & D_{66}^s & 0 & 0 & H_{66}^s & 0 \\ X_{13} & X_{23} & 0 & Y_{13} & Y_{23} & 0 & Y_{13}^s & Y_{23}^s & 0 & Z_{33} \end{bmatrix} \begin{pmatrix} \epsilon_x^0 \\ \epsilon_y^0 \\ \gamma_{xy}^0 \\ k_x^b \\ k_y^b \\ k_{xy}^b \\ k_x^s \\ k_y^s \\ k_{xy}^s \\ \epsilon_z^0 \end{pmatrix} \tag{19a}$$

$$\begin{Bmatrix} S_{yz}^s \\ S_{xz}^s \end{Bmatrix} = \begin{bmatrix} A_{44}^s & 0 \\ 0 & A_{55}^s \end{bmatrix} \begin{Bmatrix} \gamma_{yz}^0 \\ \gamma_{xz}^0 \end{Bmatrix} \tag{19b}$$

where the stiffness components and inertias are given as:

$$(A_{ij}, A_{ij}^s, B_{ij}, D_{ij}, B_{ij}^s, D_{ij}^s, H_{ij}^s) = \int_{-h/2}^{h/2} Q_{ij} (1, g^2(z), z, z^2, f(z), z f(z), f^2(z)) dz \tag{20a}$$

$$(X_{ij}, Y_{ij}, Y_{ij}^s, Z_{ij}) = \int_{-h/2}^{h/2} (1, z, f(z), g'(z)) g'(z) Q_{ij} dz \tag{20b}$$

$$(I_0, I_1, I_2, J_1, J_2, J_0, K_0, K_2) = \int_{-h/2}^{h/2} (1, z, z^2, f, z f, g, g^2, f^2) \rho(z) dz \tag{20c}$$

and $\rho(z)$ is the mass density.

The in-plane normal and shear stresses (σ_x, σ_y and τ_{xy}) can be determined accurately by the constitutive Equation (10) for FG plates. However, if the transverse normal and shear stresses (σ_z, τ_{yz} and τ_{xz}) are computed from the constitutive Equation (10), they may not respect the boundary conditions at the upper and lower surfaces of the plate. Therefore, these stresses are determined by integrating the equilibrium equations of 3D elasticity with respect to thickness coordinates as:

$$\tau_{xz} = - \int_{-h/2}^z \left(\frac{\partial \sigma_x}{\partial x} + \frac{\partial \tau_{xy}}{\partial y} \right) dz + C_1(x, y) \tag{21a}$$

$$\tau_{yz} = - \int_{-h/2}^z \left(\frac{\partial \tau_{xy}}{\partial x} + \frac{\partial \sigma_y}{\partial y} \right) dz + C_2(x, y) \tag{21b}$$

$$\sigma_z = - \int_{-h/2}^z \left(\int_{-h/2}^z \left[\frac{\partial^2 \sigma_x}{\partial x^2} + 2 \frac{\partial^2 \tau_{xy}}{\partial x \partial y} + \frac{\partial^2 \sigma_y}{\partial y^2} \right] dz \right) dz + C_3(x, y)z + C_4(x, y) \tag{21c}$$

where C_i 's ($i = 1, 4$) are constants and are determined by the following boundary conditions at the upper and lower surfaces of the plate.

$$\tau_{xz}|_{z=\pm h/2} = 0, \tau_{yz}|_{z=\pm h/2} = 0, \sigma_z|_{z=h/2} = q(x, y), \sigma_z|_{z=-h/2} = 0 \tag{21d}$$

3. Closed-Form Solutions for Simply Supported FG Plates

The Navier's procedure [18,57], based on double Fourier series, is employed herein to define the closed-form solution of the partial differential equations (Equation (18)) for which the displacement variables satisfying the boundary conditions can be given as

$$\begin{pmatrix} u_0 \\ v_0 \\ w_0 \\ \theta \\ \phi_z \end{pmatrix} = \sum_{m=1}^{\infty} \sum_{n=1}^{\infty} \begin{pmatrix} U_{mn} \cos(\alpha x) \sin(\beta y) \\ V_{mn} \sin(\alpha x) \cos(\beta y) \\ W_{mn} \sin(\alpha x) \sin(\beta y) \\ X_{mn} \sin(\alpha x) \sin(\beta y) \\ \phi_{mn} \sin(\alpha x) \sin(\beta y) \end{pmatrix} \tag{21e}$$

where $(U_{mn}, V_{mn}, W_{mn}, X_{mn}, \phi_{mn})$ are unknown functions to be determined. α and β are expressed as:

$$\alpha = m\pi/a \text{ and } \beta = n\pi/b \tag{22}$$

The transverse distributed load $q(x, y)$ is also expanded in a double Fourier series as

$$q(x, y) = \sum_{m=1}^{\infty} \sum_{n=1}^{\infty} q_{mn} \sin\left(\frac{m\pi}{a}x\right) \sin\left(\frac{n\pi}{b}y\right) \tag{23}$$

The coefficients q_{mn} are given below for some general loadings:

- For uniformly distributed load

$$q_{mn} = \begin{cases} \frac{16q_0}{mn\pi^2}, & m, n = 1, 3, 5, \dots \\ 0 & m, n = 2, 4, 6, \dots \end{cases} \tag{24}$$

- For sinusoidal distributed load

$$q_{mn} = q_0 \tag{25}$$

in which q_0 is the intensity of the load.

Substituting Equations (19) and (23) into Equation (18), closed-form solutions of static problem of FG plate can be obtained as follows:

$$\begin{bmatrix} S_{11} & S_{12} & S_{13} & S_{14} & S_{15} \\ S_{12} & S_{22} & S_{23} & S_{24} & S_{25} \\ S_{13} & S_{23} & S_{33} & S_{34} & S_{35} \\ S_{14} & S_{24} & S_{34} & S_{44} & S_{45} \\ S_{15} & S_{25} & S_{35} & S_{45} & S_{55} \end{bmatrix} \begin{pmatrix} U_{mn} \\ V_{mn} \\ W_{mn} \\ X_{mn} \\ \phi_{mn} \end{pmatrix} = \begin{pmatrix} 0 \\ 0 \\ q_{mn} \\ 0 \\ 0 \end{pmatrix} \tag{26}$$

in which S_{ij} are the stiffness matrix's coefficients and are defined as follows:

$$\begin{aligned}
 S_{11} &= \alpha^2 B_{11} + \beta^2 A_{66} \\
 S_{12} &= \alpha\beta(A_{12} + A_{66}) \\
 S_{13} &= -\alpha^3 B_{11} - \alpha\beta^2(B_{12} + 2B_{66}) \\
 S_{14} &= -\alpha(k_1 B_{11}^s + k_2 B_{12}^s) + \alpha\beta^2 B_{66}^s(k_1 A' + k_2 B') \\
 S_{15} &= \alpha X_{13} \\
 S_{22} &= \alpha^2 A_{66} + \beta^2 A_{22} \\
 S_{23} &= -\beta^3 B_{22} - \alpha^2\beta(B_{12} + 2B_{66}) \\
 S_{24} &= -\beta(k_1 B_{12}^s + k_2 B_{22}^s) + \alpha^2\beta(k_1 A' + k_2 B')B_{66}^s \\
 S_{25} &= -\beta X_{23} \\
 S_{33} &= \alpha^4 D_{11} + \beta^4 D_{22} + 2\alpha^2\beta^2(D_{12} + 2D_{66}) \\
 &\quad + K_w + K_s(\alpha^2 + \beta^2) \\
 S_{34} &= \alpha^2 k_1 D_{11}^s + (k_2 \alpha^2 + k_1 \beta^2) D_{12}^s + \beta^2 k_2 D_{22}^s \\
 &\quad - 2\alpha^2 \beta^2 (k_1 A' + k_2 B') D_{66}^s \\
 S_{35} &= \alpha^2 Y_{13} + \beta^2 Y_{23} \\
 S_{44} &= k_1^2 H_{11}^s + k_2^2 H_{22}^s + 2k_1 k_2 H_{12}^s + \alpha^2 \beta^2 (k_1 A' + k_2 B')^2 H_{66}^s \\
 &\quad + \alpha^2 (k_1 A')^2 A_{55}^s + \beta^2 (k_2 B')^2 A_{44}^s \\
 S_{45} &= k_1 Y_{13}^s + k_2 Y_{23}^s + \alpha^2 k_1 A' A_{55}^s + \beta^2 k_2 B' A_{44}^s \\
 S_{55} &= \alpha^2 A_{55}^s + \beta^2 A_{44}^s + Z_{33}
 \end{aligned} \tag{27}$$

4. Results and Discussion

4.1. Bending Analysis of Simply Supported FG Plates

In this section, different numerical examples are presented and compared to the results of various 2D, 3D, and quasi-3D shear deformation theories to check the accuracy of the present theory in investigating the bending behaviour of simply supported FG plates. The mechanical characteristics of the metal and ceramics used in this study are given in Table 1. In the calculations, both homogeneous isotropic plates and FGPs are studied. Additionally, an analysis of the parameters was performed. For convenience, the following non-dimensional displacements and stresses are used in presenting the numerical results in graphical and tabular forms:

$$\begin{aligned}
 \bar{w} &= \frac{10h^3 E_c}{a^4 q_0} w\left(\frac{a}{2}, \frac{b}{2}, z\right), \bar{\sigma}_x = \frac{h}{aq_0} \sigma_x\left(\frac{a}{2}, \frac{b}{2}, z\right), \bar{\sigma}_y = \frac{h}{aq_0} \sigma_y\left(\frac{a}{2}, \frac{b}{2}, z\right), \\
 \bar{\tau}_{xy} &= \frac{h}{aq_0} \tau_{xy}(0, 0, z), \bar{\tau}_{xz} = \frac{h}{aq_0} \tau_{xz}\left(0, \frac{b}{2}, z\right), \bar{\tau}_{yz} = \frac{h}{aq_0} \tau_{yz}\left(\frac{a}{2}, 0, z\right) \\
 \tilde{u} &= \frac{E_c}{hq_0} u\left(0, \frac{b}{2}, z\right), \tilde{w} = \frac{E_c}{hq_0} w\left(\frac{a}{2}, \frac{b}{2}, z\right), \tilde{\sigma}_x = \frac{\sigma_x\left(\frac{a}{2}, \frac{b}{2}, z\right)}{q_0}, \\
 \tilde{\sigma}_z &= \frac{\sigma_z\left(\frac{a}{2}, \frac{b}{2}, z\right)}{q_0}, \tilde{\tau}_{xy} = \frac{\tau_{xy}(0, 0, z)}{q_0}, \tilde{\tau}_{xz} = \frac{\tau_{xz}\left(0, \frac{b}{2}, z\right)}{q_0} \\
 \hat{u} &= \frac{G_1}{hq_0} u\left(0, \frac{b}{2}, z\right), \hat{w} = \frac{G_1}{hq_0} w\left(\frac{a}{2}, \frac{b}{2}, z\right),
 \end{aligned} \tag{28}$$

Table 1. Material properties used in the FG plates [52,55].

Material	Properties		
	E (GPa)	V	ρ (kg/m ³)
Aluminum (Al)	70	0.3	2702
Alumina (Al ₂ O ₃)	380	0.3	3800
Zirconia (ZrO ₂)	200	0.3	5700

4.1.1. Functionally Graded Plates (P-FGM)

In this section, non-dimensional displacements and stresses of an Al/Al_2O_3 FG square plate under uniformly and sinusoidal distributed loads for various values of the power law index are calculated and presented in Tables 2 and 3.

Table 2. The non-dimensional displacement and stress components of an Al/Al_2O_3 FG square plate subjected to uniformly distributed load ($a/h = 10$).

k	Theory	ϵ_z	$\bar{w}(0)$	$\bar{\sigma}_x(\frac{h}{2})$	$\bar{\sigma}_y(\frac{h}{3})$	$\bar{\tau}_{xz}(0)$	$\bar{\tau}_{yz}(\frac{h}{6})$	$\bar{\tau}_{xy}(-\frac{h}{3})$
0	Akavci and Tanrikulu [31]	= 0	0.4665	2.8909	1.9103	0.4988	0.4363	1.2857
	Akavci and Tanrikulu [31]	≠ 0	0.4635	2.9981	1.8925	0.4782	0.4315	1.2578
	Younsi et al. [39]	= 0	0.4665	2.8913	1.9102	0.5043	0.4367	1.2855
	Younsi et al. [39]	≠ 0	0.4637	2.9919	1.8932	0.5042	0.4317	1.2585
	Present study	= 0	0.4665	2.8912	1.9102	0.5043	0.4369	1.2856
	Present study	≠ 0	0.4625	3.0729	1.8756	0.4761	0.4307	1.2548
1	Akavci and Tanrikulu [31]	= 0	0.9288	4.4707	2.1693	0.4988	0.5364	1.1141
	Akavci and Tanrikulu [31]	≠ 0	0.8977	4.6110	2.0822	0.4782	0.5119	1.0211
	Younsi et al. [39]	= 0	0.9287	4.4713	2.1692	0.5043	0.5370	1.1141
	Younsi et al. [39]	≠ 0	0.8980	4.6005	2.0832	0.4791	0.5121	1.0225
	Present study	= 0	0.9287	4.4713	2.1692	0.5042	0.5372	1.1141
	Present study	≠ 0	0.8961	4.7379	2.0578	0.4761	0.5114	1.0206
2	Akavci and Tanrikulu [31]	= 0	1.1940	5.2248	2.0342	0.4581	0.5643	0.9909
	Akavci and Tanrikulu [31]	≠ 0	1.1376	5.3825	1.9257	0.4524	0.5081	0.8921
	Younsi et al. [39]	= 0	1.1940	5.2256	2.0340	0.4637	0.5657	0.9908
	Younsi et al. [39]	≠ 0	1.1380	5.3726	1.9281	0.4532	0.5082	0.8926
	Present study	= 0	1.1940	5.2255	2.0340	0.4636	0.5658	0.9908
	Present study	≠ 0	1.1352	5.5232	1.8972	0.4505	0.5074	0.8902
4	Akavci and Tanrikulu [31]	= 0	1.3888	5.8855	1.7205	0.4090	0.5253	1.0305
	Akavci and Tanrikulu [31]	≠ 0	1.3259	6.0382	1.6062	0.4358	0.4804	0.9274
	Younsi et al. [39]	= 0	1.3890	5.8866	1.7202	0.4151	0.5278	1.0303
	Younsi et al. [39]	≠ 0	1.3262	6.0301	1.6101	0.4365	0.4806	0.9279
	Present study	= 0	1.3889	5.8865	1.7202	0.4149	0.5279	1.0303
	Present study	≠ 0	1.3237	6.1920	1.5744	0.4341	0.4797	0.9256
10	Akavci and Tanrikulu [31]	= 0	1.5875	7.3617	1.2828	0.4436	0.4159	1.0705
	Akavci and Tanrikulu [31]	≠ 0	1.5453	7.5123	1.2016	0.4332	0.4561	0.9860
	Younsi et al. [39]	= 0	1.5875	7.3628	1.2825	0.4495	0.4174	1.0703
	Younsi et al. [39]	≠ 0	1.5454	7.5064	1.2059	0.4339	0.4562	0.9862
	Present study	= 0	1.5875	7.3628	1.2825	0.4495	0.4176	1.0703
	Present study	≠ 0	1.5436	7.6914	1.1724	0.4314	0.4554	0.9852

Table 3. Non-dimensional displacement and stress of an Al/Al₂O₃ FG square plate subjected to sinusoidal load.

<i>k</i>	Theory	ϵ_z	$\bar{\sigma}_x(h/3)$			$\bar{w}(0)$		
			<i>a/h</i> = 4	<i>a/h</i> = 10	<i>a/h</i> = 100	<i>a/h</i> = 4	<i>a/h</i> = 10	<i>a/h</i> = 100
1	Carrera et al. [21]	≠ 0	0.6221	1.5064	14.9690	0.7171	0.5875	0.5625
	Neves et al. [22]	≠ 0	0.5925	1.4945	14.9690	0.6997	0.5845	0.5624
	Neves et al. [23]	≠ 0	0.5910	1.4917	14.9440	0.7020	0.5868	0.5648
	Hebali et al. [2]	≠ 0	0.5952	1.4954	14.9630	0.6910	0.5686	0.5452
	Akavci and Tanrikulu [31]	= 0	0.5806	1.4895	14.9670	0.7282	0.5889	0.5625
	Akavci and Tanrikulu [31]	≠ 0	0.5754	1.4322	14.3060	0.6908	0.5691	0.5457
	Younsi et al. [39]	= 0	0.5808	1.4896	14.9675	0.7283	0.5889	0.5625
	Younsi et al. [39]	≠ 0	0.5758	1.4330	14.3135	0.6910	0.5692	0.5459
	Present study	= 0	0.5803	1.4894	14.9675	0.7280	0.5889	0.5625
	Present study	≠ 0	0.5705	1.4157	14.1330	0.6896	0.5680	0.5447
4	Carrera et al. [21]	≠ 0	0.4877	1.1971	11.9230	1.1585	0.8821	0.8286
	Neves et al. [22]	≠ 0	0.4404	1.1783	11.9320	1.1178	0.8750	0.8286
	Neves et al. [23]	≠ 0	0.4340	1.1593	11.7380	1.1095	0.8698	0.8241
	Hebali et al. [2]	≠ 0	0.4507	1.1779	11.8710	1.0964	0.8413	0.7926
	Akavci and Tanrikulu [31]	= 0	0.4431	1.1787	11.9200	1.1613	0.8818	0.8287
	Akavci and Tanrikulu [31]	≠ 0	0.4247	1.1017	11.0880	1.0983	0.8417	0.7925
	Younsi et al. [39]	= 0	0.4437	1.1789	11.9209	1.1609	0.8817	0.8287
	Younsi et al. [39]	≠ 0	0.4260	1.1045	11.1152	1.0982	0.8419	0.7928
	Present study	= 0	0.4424	1.1783	11.9208	1.1618	0.8818	0.8287
	Present study	≠ 0	0.4181	1.0802	10.8633	1.0970	0.8403	0.7910
10	Carrera et al. [21]	≠ 0	0.3965	0.8965	8.9077	1.3745	1.0072	0.9361
	Neves et al. [22]	≠ 0	0.3227	1.1783	11.9320	1.3490	0.8750	0.8286
	Neves et al. [23]	≠ 0	0.3108	0.8467	8.6013	1.3327	0.9886	0.9228
	Hebali et al. [2]	≠ 0	0.3325	0.8889	8.9977	1.3333	0.9791	0.9114
	Akavci and Tanrikulu [31]	= 0	0.3242	0.8778	8.9059	1.3917	1.0089	0.9362
	Akavci and Tanrikulu [31]	≠ 0	0.3095	0.8229	8.3185	1.3352	0.9818	0.9141
	Younsi et al. [39]	= 0	0.3248	0.8780	8.9059	1.3915	1.0088	0.9362
	Younsi et al. [39]	≠ 0	0.3109	0.8259	8.3473	1.3353	0.9819	0.9141
	Present study	= 0	0.3235	0.8775	8.9059	1.3917	1.0089	0.9362
	Present study	≠ 0	0.3033	0.8031	8.1118	1.3333	0.9807	0.9130

In Table 2, the computed results of non-dimensional deflection and stress components of moderately thick square FG plate under uniform load are compared to those given by quasi-3D and 2D shear deformation theories by Akavci and Tanrikulu [31] and Younsi et al. [39]. From this table, it can be observed that the results of the proposed 2D theory agree well with those of Akavci and Tanrikulu [31] and Younsi et al. [39] in all cases. Additionally, by comparing the obtained values of the present quasi-3D theory with those given by the other quasi-3D theories, an excellent correlation can be noted.

Table 3 presents the non-dimensional normal stress ($\bar{\sigma}_x$) and transverse displacement (\bar{w}) of square thin and thick plates subjected to sinusoidal load for three different power law indices (*k*). The determined results are compared with those generated by Carrera et al. [21]

based on fourth-order variations of both in-plane and transverse displacements across the thickness, quasi-3D sinusoidal and hyperbolic shear deformation theories of Neves et al. [22,23], quasi-3D shear deformation theories of Hebali et al. [2], and 2D and quasi-3D hyperbolic shear deformation theories of Akavci and Tanrikulu [31] and Younsi et al. [39]. A good agreement between the results is found for both thin and thick plates. Additionally, the present model provides a good prediction of both displacement and stress even in thick FG plates, where the stretching effects are more pronounced.

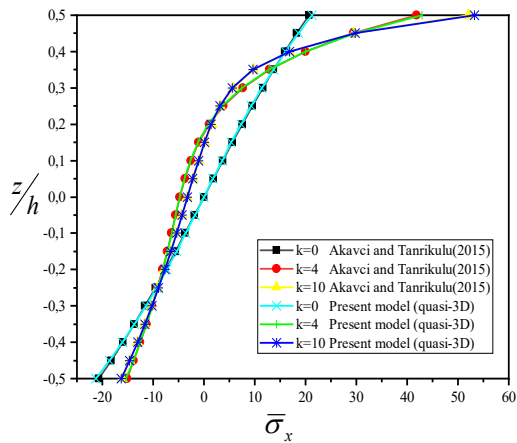
Moreover, it should be noticed that the number of unknown variables used in the present formulation is just four in the 2D theory and five in the quasi-3D model, while nine unknown functions were used in hyperbolic shear deformation theories of Neves et al. [22,23]. It can be concluded that the present theory is not only accurate but also comparatively simple in predicting the bending response of simply supported FGM plates.

The stresses and displacements variations through the thickness of Al/Al₂O₃ FG square plate subjected to sinusoidal load are plotted in Figure 2. The results are shown as compared to the quasi-3D shear deformation theory of Akavci and Tanrikulu [31] for different values of the power law index (k). From this figure, excellent agreement between the obtained results and those computed by Akavci and Tanrikulu can be observed [31]. It is important to note that the in-plane stresses ($\bar{\sigma}_x$) and ($\bar{\tau}_{xy}$) exhibit linear variation through the thickness of homogeneous plate, while variation is parabolic for FG plates. The figure also shows that the deflection (\bar{w}) and in-plane stresses—($\bar{\sigma}_x$) and ($\bar{\sigma}_z$), respectively—increase and that the shear stresses ($\bar{\tau}_{xy}$) and ($\bar{\tau}_{xz}$) decrease with the increasing value of material index (k).

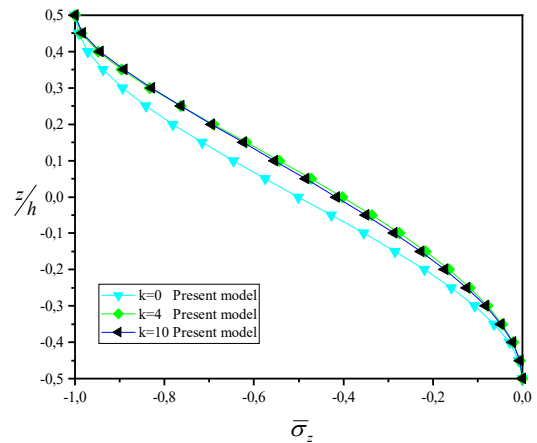
In the middle of the FG plate, the axial stresses are negative in the lower half of the metal for all values of the power index k and then become positive in the upper part starting from the geometric ratio $z/h > 0.17$. Beyond this value, the stresses tend to increase with the increase in the power index, and the most important stress is found for $k = 10$. An inverse behaviour is observed for the tangential stresses in the plane; they are positive and are obtained in the lower face of the plate, whereas the minimal tangential stresses are obtained on the upper face of the plate FG. The importance of these stresses depends on the quality of the air of FGM materials.

The maximum transverse shear stresses are located in the median plane for homogeneous plates, and they tend to shift slightly towards the upper surface with respect to the median plane with the importance of k . The maximum transverse shear stresses will possess an asymmetric characteristic through the thickness of the FG plate. In this case and for an index $k = 1$ the maximum axial and shear stresses in the plan are found respectively 12 and 6 times more important than the maximum transverse shear stress. Regarding the deflection (\bar{w}), it is found to be almost stable through the thickness of the plate and increases significantly proportionally with the index k .

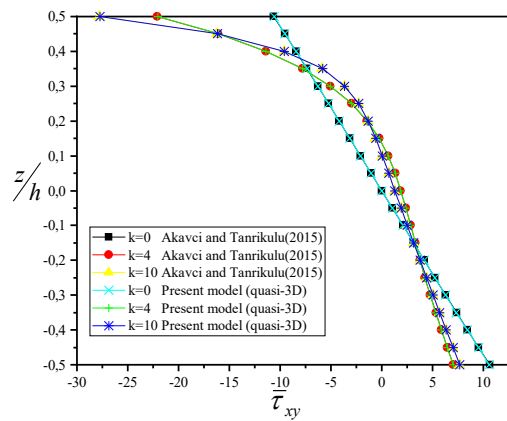
Figure 3 presents a 3D interaction diagram of the power-law index (k), side-to-thickness ratio (a/h), and centre deflection (\bar{w}) using the proposed 2D and quasi-3D theories. It can be seen from this figure that the centre deflection increases with the increase of the power law index and decreases with the increasing of the thickness ratio. It is due to the fact that a higher value of (k) corresponds to lower value of volume fraction of the ceramic phase and thus leads to the decrease of the value of the elasticity modulus, which makes the plate softer. The figure shows also that the centre deflections computed from the present 2D theory, which neglects the thickness stretching effect, are higher than those calculated from quasi-3D theory.



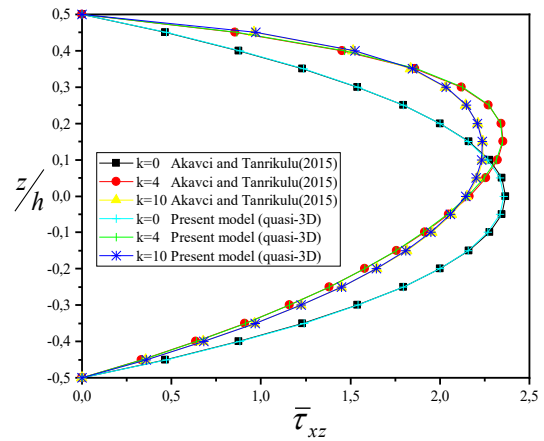
(a): ($\bar{\sigma}_x$) versus z/h



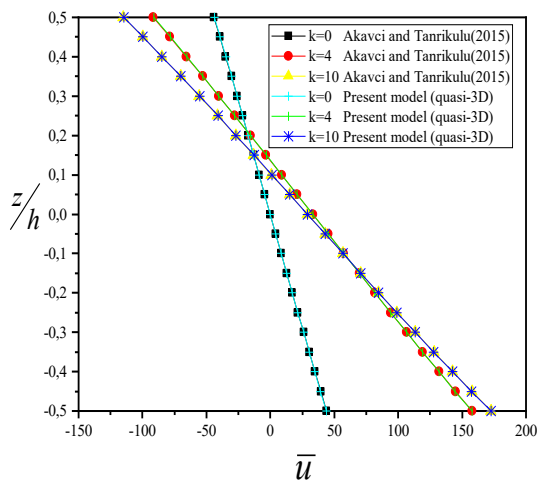
(b): ($\bar{\sigma}_z$) versus z/h



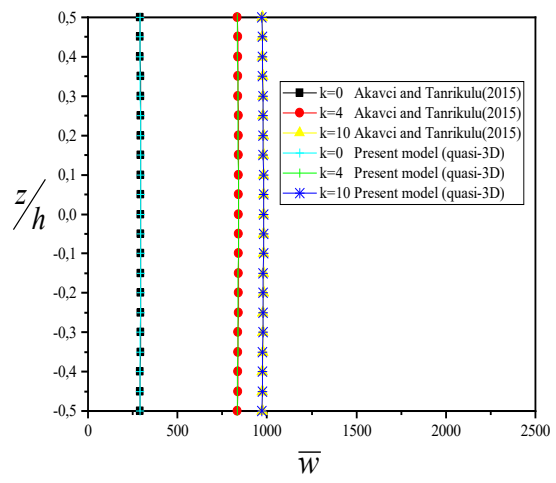
(c): ($\bar{\tau}_{xy}$) versus z/h



(d): ($\bar{\tau}_{xz}$) versus z/h



(e): (\bar{u}) versus z/h



(f): (\bar{w}) versus z/h

Figure 2. Distributions of the non-dimensional displacements (\bar{u}, \bar{w}) and stresses ($\bar{\sigma}_x, \bar{\sigma}_z, \bar{\tau}_{xy}, \bar{\tau}_{xz}$) through the thickness of square P-GM plate ($a/h = 10$) [31].

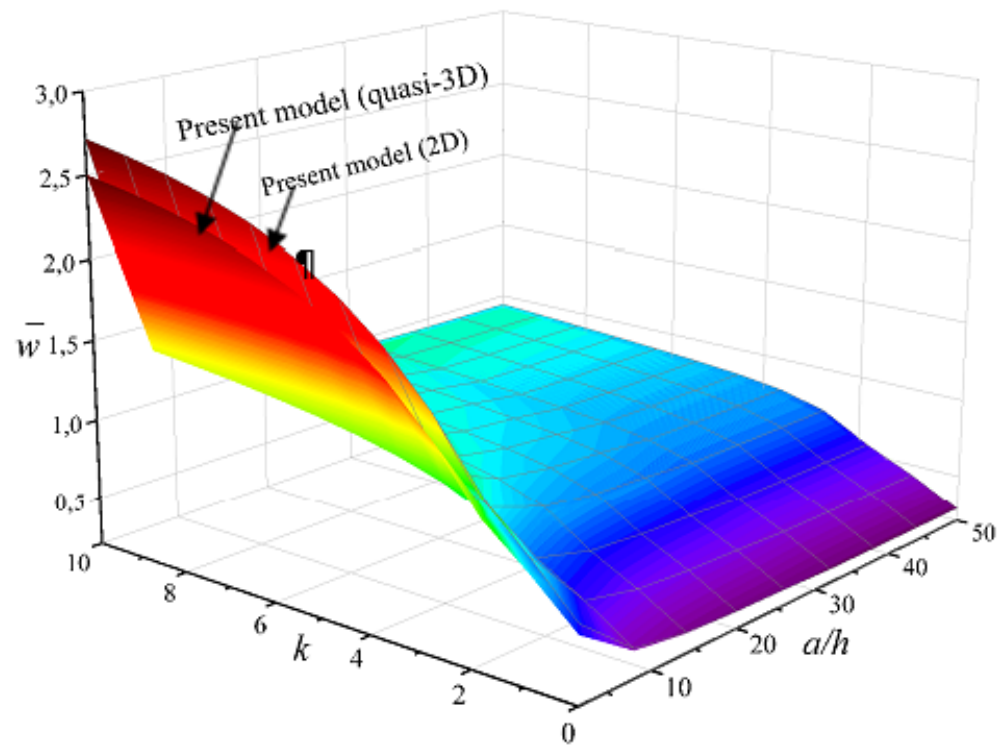


Figure 3. Effect of the power law index k and side-to-thickness ratio a/h on the non-dimensional deflection \bar{w} of simply supported Al/Al_2O_3 P-FGM plates.

4.1.2. Exponentially Graded Plates (E-FGM)

Computations in this section are carried out for a simply supported E-FGM plate. The material properties of the E-FGM plate are defined by the exponential function given in Equation (2). The non-dimensional stress and displacements of the E-FGM plate are calculated and compared with the results of different HSDTs for different loadings.

The centre deflections (\bar{w}) in-plane and transverse shear stresses ($\bar{\sigma}_x, \bar{\tau}_{xy}$) of Al/Al_2O_3 plates under sinusoidal loads are calculated for different values of aspect ratio (b/a), thickness ratio (a/h), and exponent values (k) in Tables 4–7. The central deflections of the very thick E-FGM plates are analysed in Table 4. The obtained predictions are compared with the quasi-3D sinusoidal and exact 3D elasticity theories of Zenkour [19], 2D and quasi-3D trigonometric models of Mantari and Soares [26], and the quasi-3D and 2D shear deformation theories by Akavci and Tanrikulu [31], Younsi et al. [39]. Since the proposed and other quasi-3D models include the thickness-stretching influence, they lead to results close to each other, whereas 2D HSDTs overestimate the deflections due to omitting the thickness-stretching influence. In Tables 5 and 6, the computed non-dimensional stresses are provided as compared with those given by Younsi et al. [39], Akavci and Tanrikulu [31] based on quasi-3D and 2D hyperbolic theories and Mantari and Soares [26] using 2D and quasi-3D trigonometric theories. It can be seen from the table that an excellent agreement is achieved between the results of present theory and those of other theories. Tables 4–7 also demonstrate that deflection (\bar{w}) and transverse shear stress ($\bar{\tau}_{xz}$) decrease and that in-plane stress ($\bar{\sigma}_x$) increases with an increase in the exponent (k).

Table 4. Non-dimensional deflection $\bar{w}(0) = \frac{10h^3 E_0}{a^4 q_0} w\left(\frac{a}{2}, \frac{b}{2}, 0\right)$ of E-FGM plates subjected to sinusoidal distributed load ($a/h = 2$).

<i>b/a</i>	Theory	ϵ_z	<i>k</i>					
			0.1	0.3	0.5	0.7	1	1.5
1	Zenkour [19]	$\neq 0$	0.5769	0.5247	0.4766	0.4324	0.3726	0.2890
	Zenkour [19]	$= 0$	0.5730	0.5180	0.4678	0.4221	0.3611	0.2771
	Mantari and Soares [26]	$\neq 0$	0.5778	0.5224	0.4717	0.4256	0.3648	0.2793
	Mantari and Soares [26]	$= 0$	0.6362	0.5751	0.5194	0.4687	0.4017	0.3079
	Akavci and Tanrikulu [31]	$= 0$	0.6351	0.5741	0.5185	0.4679	0.4004	0.3075
	Akavci and Tanrikulu [31]	$\neq 0$	0.5750	0.5198	0.4694	0.4236	0.3624	0.2780
	Younsi et al. [39]	$= 0$	0.6355	0.5745	0.5189	0.4683	0.4007	0.3077
	Younsi et al. [39]	$\neq 0$	0.5758	0.5205	0.4701	0.4242	0.3629	0.2784
	Present study	$= 0$	0.6343	0.5734	0.5179	0.4674	0.4000	0.3072
	Present study	$\neq 0$	0.5731	0.5181	0.4679	0.4222	0.3612	0.2771
2	Zenkour [19]	$\neq 0$	1.1944	1.0859	0.9864	0.8952	0.7726	0.6017
	Zenkour [19]	$= 0$	1.1879	1.0739	0.9700	0.8754	0.7493	0.5757
	Mantari and Soares [26]	$\neq 0$	1.1940	1.0794	0.9750	0.8799	0.7537	0.5786
	Mantari and Soares [26]	$= 0$	1.2776	1.1553	1.0441	0.9430	0.8092	0.6237
	Akavci and Tanrikulu [31]	$= 0$	1.2763	1.1541	1.0431	0.9422	0.8079	0.6234
	Akavci and Tanrikulu [31]	$\neq 0$	1.1938	1.0765	0.9723	0.8775	0.7511	0.5771
	Younsi et al. [39]	$= 0$	1.2768	1.1546	1.0435	0.9426	0.8082	0.6236
	Younsi et al. [39]	$\neq 0$	1.1917	1.0774	0.9731	0.8782	0.7517	0.5775
	Present study	$= 0$	1.2753	1.1532	1.0423	0.9415	0.8074	0.6231
	Present study	$\neq 0$	1.1880	1.0740	0.9701	0.8755	0.7494	0.5758
3	Zenkour [19]	$\neq 0$	1.4429	1.3116	1.1912	1.0811	0.9333	0.7275
	Zenkour [19]	$= 0$	1.4354	1.2977	1.1722	1.0579	0.9056	0.6961
	Mantari and Soares [26]	$\neq 0$	1.4421	1.3037	1.1776	1.0627	0.9104	0.6992
	Mantari and Soares [26]	$= 0$	1.5340	1.3873	1.2540	1.1329	0.9725	0.7506
	Akavci and Tanrikulu [31]	$= 0$	1.5327	1.3861	1.2530	1.1320	0.9712	0.7503
	Akavci and Tanrikulu [31]	$\neq 0$	1.4386	1.3005	1.1748	1.0602	0.9076	0.6976
	Younsi et al. [39]	$= 0$	1.5332	1.3866	1.2534	1.1324	0.9715	0.7504
	Younsi et al. [39]	$\neq 0$	1.4396	1.3015	1.1756	1.0610	0.9082	0.6981
	Present study	$= 0$	1.5316	1.3852	1.2521	1.1313	0.9706	0.7499
	Present study	$\neq 0$	1.4354	1.2977	1.1722	1.0579	0.9057	0.6961

In Figure 4, the variations of non-dimensional displacements and stresses according to the thickness of an E-FGM plate subjected to sinusoidal loading for different E_c/E_m ratios are displayed using the present theory, including the thickness-stretching effect and compared to the quasi-3D theory of Younsi et al. [39]. A very good accuracy between the solutions is observed. It can be seen also from these results that the non-dimensional displacements increase with the increasing of E_c/E_m . In addition, it can be deduced that E_c/E_m ratios affect considerably the non-dimensional stresses.

Table 5. Non-dimensional stress $\bar{\sigma}_x\left(\frac{h}{2}\right) = \frac{h^2}{a^2q_0}\sigma_x\left(\frac{a}{2}, \frac{b}{2}, \frac{h}{2}\right)$ of E-FGM plates subjected to sinusoidal distributed load ($a/h = 10$).

<i>b/a</i>	Theory	ϵ_z	<i>k</i>								
			0.1	0.3	0.5	0.7	1	1.5	2	2.5	3
1	Mantari and Soares [26]	$\neq 0$	0.2196	0.2345	0.2503	0.2671	0.2944	0.3460	0.4065	0.4775	0.5603
	Mantari and Soares [26]	$= 0$	0.2062	0.2204	0.2355	0.2515	0.2774	0.3264	0.3835	0.4502	0.5278
	Akavci and Tanrikulu [31]	$= 0$	0.2063	0.2205	0.2356	0.2516	0.2776	0.3266	0.3838	0.4504	0.5281
	Akavci and Tanrikulu [31]	$\neq 0$	0.2142	0.2285	0.2438	0.2601	0.2866	0.3370	0.3964	0.4664	0.5485
	Younsi et al. [39]	$= 0$	0.2063	0.2205	0.2355	0.2516	0.2775	0.3265	0.3837	0.4504	0.5279
	Younsi et al. [39]	$\neq 0$	0.2137	0.2280	0.2433	0.2595	0.2860	0.3363	0.3957	0.4657	0.5478
	Present study	$= 0$	0.2063	0.2205	0.2356	0.2517	0.2776	0.3266	0.3838	0.4505	0.5282
	Present study	$\neq 0$	0.2195	0.2344	0.2502	0.2670	0.2943	0.4359	0.4064	0.4773	0.5602
2	Mantari and Soares [26]	$\neq 0$	0.4552	0.4867	0.5200	0.5554	0.6126	0.7201	0.8449	0.9898	1.1580
	Mantari and Soares [26]	$= 0$	0.4350	0.4649	0.4966	0.5303	0.5850	0.6881	0.8085	0.9490	1.1125
	Akavci and Tanrikulu [31]	$= 0$	0.4351	0.4650	0.4968	0.5305	0.5852	0.6884	0.8088	0.9493	1.1129
	Akavci and Tanrikulu [31]	$\neq 0$	0.4466	0.4773	0.5098	0.5443	0.6002	0.7058	0.8289	0.9725	1.1397
	Younsi et al. [39]	$= 0$	0.4351	0.4650	0.4967	0.5305	0.5851	0.6883	0.8087	0.9492	1.1128
	Younsi et al. [39]	$\neq 0$	0.4459	0.4765	0.5090	0.5435	0.5993	0.7048	0.8278	0.9728	1.1388
	Present study	$= 0$	0.4351	0.4650	0.4968	0.5306	0.5852	0.6884	0.8089	0.9494	1.1131
	Present study	$\neq 0$	0.4551	0.4865	0.5199	0.5553	0.6124	0.7199	0.8447	0.9897	1.1579
3	Mantari and Soares [26]	$\neq 0$	0.5514	0.5896	0.6302	0.6733	0.7427	0.8730	1.0240	1.1990	1.4017
	Mantari and Soares [26]	$= 0$	0.5288	0.5651	0.6037	0.6447	0.7112	0.8365	0.9828	1.1536	1.3523
	Akavci and Tanrikulu [31]	$= 0$	0.5290	0.5653	0.6039	0.6449	0.7114	0.8368	0.9832	1.1540	1.3528
	Akavci and Tanrikulu [31]	$\neq 0$	0.5418	0.5791	0.6187	0.6608	0.7289	0.8570	1.0061	1.1797	1.3813
	Younsi et al. [39]	$= 0$	0.5289	0.5652	0.6038	0.6449	0.7113	0.8367	0.9831	1.1538	1.3527
	Younsi et al. [39]	$\neq 0$	0.5410	0.5783	0.6179	0.6599	0.7279	0.8559	1.0050	1.1786	1.3803
	Present study	$= 0$	0.5290	0.5653	0.6039	0.6450	0.7114	0.8368	0.9833	1.1541	1.3529
	Present study	$\neq 0$	0.5512	0.5895	0.6300	0.6731	0.7425	0.8728	1.0238	1.1988	1.4016

It should be noted that the normal stress ($\bar{\sigma}_x$) increases in importance in the two extreme surfaces, whether in the ceramic or in the metal depending on the couple E_c/E_m . When $E_c/E_m = 0.1$, the compressive stress in the metal is on the order of 4.44 times greater than that of ceramic traction. An opposite behaviour occurs in the case that $E_c/E_m = 10$, in which case the compressive stress in the metal is 4.44 times less than that of the traction in the upper layer of the ceramic. When $E_c/E_m = 1$, the normal stress is asymmetrical on both sides of the middle layer of the plate. The maximum shear stresses ($\tilde{\tau}_{xy}$) are in the external layers and they are half in comparison with the normal stresses ($\bar{\sigma}_x$). It is also noted that the maximum shearing stresses through the thickness ($\tilde{\tau}_{xz}$) are four times less than the shear stresses ($\tilde{\tau}_{xy}$).

Table 6. Non-dimensional stress $\bar{\tau}_{xz}(0) = \frac{h}{a q_0} \tau_{xz}(0, \frac{b}{2}, 0)$ of E-FGM plates subjected to sinusoidal distributed load ($a/h = 10$).

<i>b/a</i>	Theory	ϵ_z	<i>k</i>								
			0.1	0.3	0.5	0.7	1	1.5	2	2.5	3
1	Mantari and Soares [26]	$\neq 0$	0.2454	0.2450	0.2442	0.2430	0.2405	0.2344	0.2263	0.2162	0.2045
	Mantari and Soares [26]	$= 0$	0.2380	0.2376	0.2368	0.2356	0.2330	0.2268	0.2185	0.2094	0.1985
	Akavci and Tanrikulu [31]	$= 0$	0.2434	0.2430	0.2422	0.2410	0.2385	0.2324	0.2242	0.2140	0.2023
	Akavci and Tanrikulu [31]	$\neq 0$	0.2367	0.2364	0.2359	0.2353	0.2338	0.2300	0.2249	0.2182	0.2102
	Younsi et al. [39]	$= 0$	0.2416	0.2412	0.2404	0.2392	0.2366	0.2305	0.2222	0.2121	0.2003
	Younsi et al. [39]	$\neq 0$	0.2371	0.2369	0.2364	0.2357	0.2342	0.2304	0.2252	0.2186	0.2105
	Present study	$= 0$	0.2461	0.2457	0.2449	0.2437	0.2412	0.2351	0.2269	0.2168	0.2051
	Present study	$\neq 0$	0.2357	0.2354	0.2350	0.2343	0.2328	0.2291	0.2240	0.2174	0.2094
2	Mantari and Soares [26]	$\neq 0$	0.3927	0.3921	0.3908	0.3889	0.3849	0.3752	0.3621	0.3460	0.3273
	Mantari and Soares [26]	$= 0$	0.3810	0.3803	0.3790	0.3770	0.3730	0.3630	0.3497	0.3344	0.3165
	Akavci and Tanrikulu [31]	$= 0$	0.3896	0.3889	0.3877	0.3857	0.3817	0.3719	0.3588	0.3425	0.3237
	Akavci and Tanrikulu [31]	$\neq 0$	0.3790	0.3787	0.3779	0.3768	0.3744	0.3684	0.3602	0.3496	0.3368
	Younsi et al. [39]	$= 0$	0.3867	0.3860	0.3847	0.3828	0.3787	0.3689	0.3557	0.3394	0.3206
	Younsi et al. [39]	$\neq 0$	0.3797	0.3793	0.3786	0.3774	0.3750	0.3691	0.3608	0.3501	0.3373
	Present study	$= 0$	0.3939	0.3933	0.3920	0.3901	0.3860	0.3763	0.3632	0.3470	0.3282
	Present study	$\neq 0$	0.3774	0.3770	0.3763	0.3752	0.3728	0.3669	0.3587	0.3482	0.3355
3	Mantari and Soares [26]	$\neq 0$	0.4418	0.4411	0.4396	0.4375	0.4330	0.4221	0.4074	0.3893	0.3683
	Mantari and Soares [26]	$= 0$	0.4286	0.4279	0.4264	0.4242	0.4196	0.4084	0.3934	0.3761	0.3558
	Akavci and Tanrikulu [31]	$= 0$	0.4383	0.4376	0.4361	0.4340	0.4294	0.4185	0.4036	0.3854	0.3642
	Akavci and Tanrikulu [31]	$\neq 0$	0.4265	0.4261	0.4252	0.4239	0.4212	0.4146	0.4053	0.3934	0.3789
	Younsi et al. [39]	$= 0$	0.4350	0.4343	0.4328	0.4307	0.4261	0.4151	0.4002	0.3819	0.3607
	Younsi et al. [39]	$\neq 0$	0.4273	0.4268	0.4260	0.4247	0.4220	0.4153	0.4059	0.3940	0.3795
	Present study	$= 0$	0.4432	0.4425	0.4410	0.4389	0.4343	0.4234	0.4086	0.3904	0.3693
	Present study	$\neq 0$	0.4246	0.4242	0.4234	0.4221	0.4194	0.4128	0.4036	0.3918	0.3775

4.1.3. Comparative Study

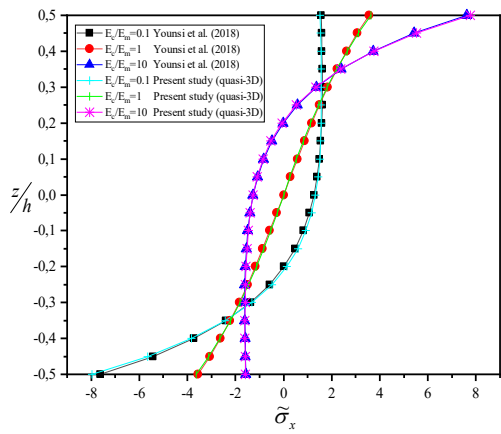
In this section, parametric studies have been presented to evaluate the effect of the power law index (*k*) and side-to-thickness ratio (*a/h*) on the bending of functionally graded plates using three rules of mixture (P-FGM, E-FGM, Mori–Tanaka models). Figure 5 illustrates the variation of non-dimensional deflection (\bar{w}) with respect to exponent index (*k*) and slenderness ratio (*a/h*) for P-FGM, E-FGM, Mori–Tanaka homogenization scheme. It can be noted from this figure, that when the exponent index increases, deflections of plates using E-FGM decrease whereas the deflections increase when P-FGM and Mori–Tanaka models are used. Such behaviour is due to the fact that the increase in the power law index will increase the stiffness of the EGM plate and thus lead to a reduction of the transverse displacement.

Table 7. Non-dimensional central displacement $\bar{w}(0) = G(h)w/h q_0$ and in-plane normal stress $\bar{\sigma}_x(0) = \sigma_x(0)/q_0$ of E-FGM plates subjected to uniformly distributed load.

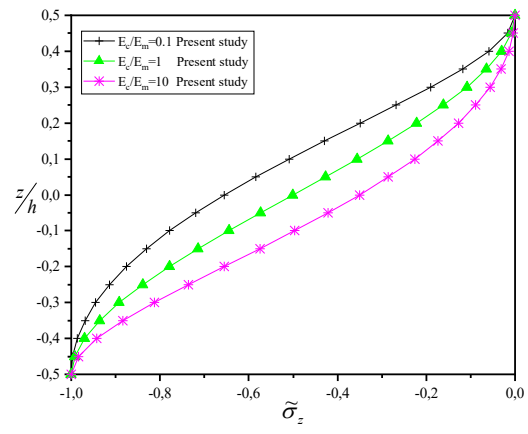
<i>h/a</i>	Quantity	Theory	E_0/E_1				
			0.1	0.5	1	2	10
0.2	\bar{w}	Vaghefi et al. [58] (BEM)	4.0916	8.9751	12.5990	17.6640	39.0600
		Vaghefi et al. [58] (FEM)	4.1215	9.0047	12.6130	17.7110	39.1550
		Akavci and Tanrikulu [31] ($\epsilon_z \neq 0$)	3.8333	8.8724	12.5970	17.7440	38.3330
		Younsi et al. [39] ($\epsilon_z \neq 0$)	3.8345	8.8756	12.6025	17.7511	38.3451
		Present study ($\epsilon_z = 0$)	4.1011	9.1087	12.8653	18.2171	41.0098
	Present study ($\epsilon_z \neq 0$)	3.8265	8.8560	12.5740	17.7123	38.2668	
	$\bar{\sigma}_x$ ($-h/2$)	Vaghefi et al. [58] (BEM)	−15.356	−9.2902	−7.4462	−5.9410	−3.4665
		Vaghefi et al. [58] (FEM)	−15.403	−9.2995	−7.4588	−5.9591	−3.4805
		Akavci and Tanrikulu [31] ($\epsilon_z \neq 0$)	−16.3220	−9.6545	−7.6944	−6.1109	−3.4530
		Younsi et al. [39] ($\epsilon_z \neq 0$)	−16.2898	−9.6313	−7.6770	−6.0994	−3.4504
Present study ($\epsilon_z = 0$)		−15.6820	−9.2913	−7.3718	−5.8141	−3.2271	
Present study ($\epsilon_z \neq 0$)	−16.6927	−9.8955	−7.8723	−6.2318	−3.4891		
0.3	\bar{w}	Vaghefi et al. [58] (BEM)	0.9707	2.1378	2.9853	4.1208	8.7134
		Vaghefi et al. [58] (FEM)	0.9732	2.1407	2.9792	4.1333	8.7293
		Akavci and Tanrikulu [31] ($\epsilon_z \neq 0$)	0.8923	2.0834	2.9602	4.1669	8.9229
		Younsi et al. [39] ($\epsilon_z \neq 0$)	0.8925	2.0843	2.9615	4.1685	8.9253
		Present study ($\epsilon_z = 0$)	0.9602	2.1772	3.0822	4.3543	9.6015
	Present study ($\epsilon_z \neq 0$)	0.8908	2.0798	2.9549	4.1595	8.9080	
	$\bar{\sigma}_x$	Vaghefi et al. [58] (BEM)	−7.223	−4.3084	−3.4496	−2.7499	−1.6449
		Vaghefi et al. [58] (FEM)	−7.2639	−4.3378	−3.4681	−2.7673	−1.6499
		Akavci and Tanrikulu [31] ($\epsilon_z \neq 0$)	−7.6576	−4.5062	−3.5748	−2.8235	−1.5731
		Younsi et al. [39] ($\epsilon_z \neq 0$)	−7.6386	−4.4941	−3.5659	−2.8175	−1.5715
Present study ($\epsilon_z = 0$)		−7.2499	−4.2796	−3.3846	−2.6589	−1.4605	
Present study ($\epsilon_z \neq 0$)	−7.7999	−4.5974	−3.6421	−2.8693	−1.5869		

Figure 6 is devoted to present the influence of side-to-thickness ratio on the non-dimensional deflection of a simply supported plate with different models. As can be observed from this figure, an increase in side-to-thickness ratio causes a reduction in the magnitude of deflection. This means that the effect of shear deformation is significant when plates are thick ($a/h \leq 5$) and negligible for thin plates. Furthermore, it is apparent that plates made with exponential function have the lowest deflection than the other functions.

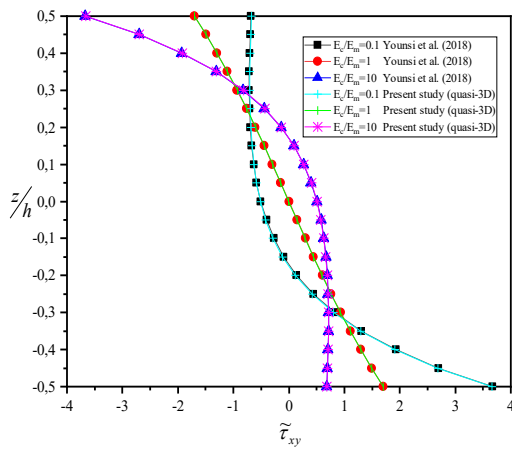
An additional comparative study for evaluating the dimensionless centre deflections of the Mori–Tanaka homogenization scheme and P-FGM and E-FGM plates subjected to sinusoidal load is also carried out. In Figure 7, it is shown that the deflection at the centre of plates with Mori–Tanaka homogenization model is larger than those of P-FGM and E-FGM plates. The E-FGM plate which has the smallest deflection is stiffer than the other FGM plates.



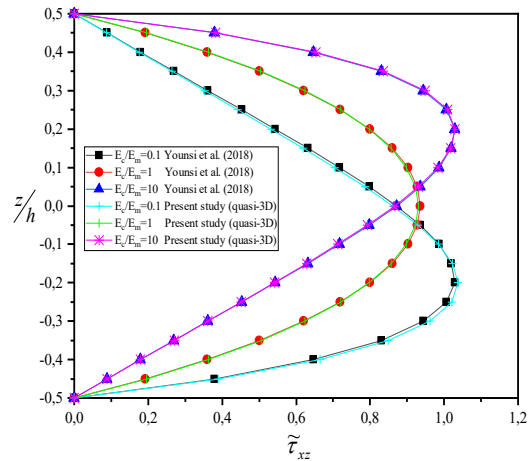
(a): ($\tilde{\sigma}_x$) versus z/h



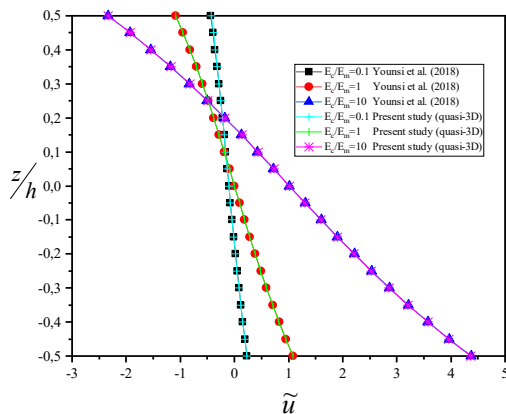
(b): ($\tilde{\sigma}_z$) versus z/h



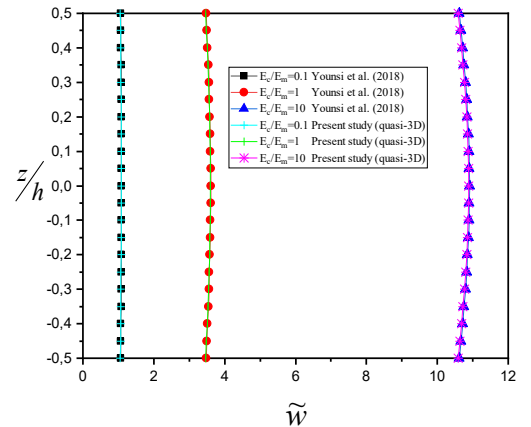
(c): ($\tilde{\tau}_{xy}$) versus z/h



(d): ($\tilde{\tau}_{xz}$) versus z/h



(e): (\tilde{u}) versus z/h



(f): (\tilde{w}) versus z/h

Figure 4. Distributions of the non-dimensional displacements (\tilde{u}, \tilde{w}) and stresses ($\tilde{\sigma}_x, \tilde{\sigma}_z, \tilde{\tau}_{xy}, \tilde{\tau}_{xz}$) through the thickness of square E-FGM plate ($a/h = 10$) [39].

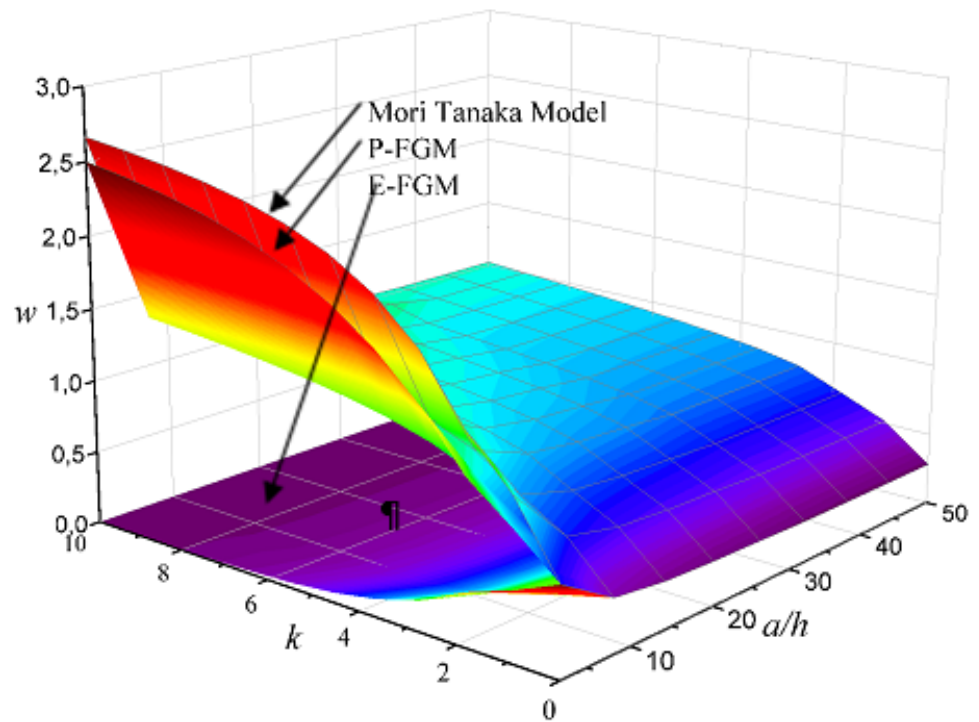


Figure 5. Non-dimensional deflection variation \bar{w} of different models of FG plates for various values of power-law index (k) and side-to-thickness ratio (a/h).

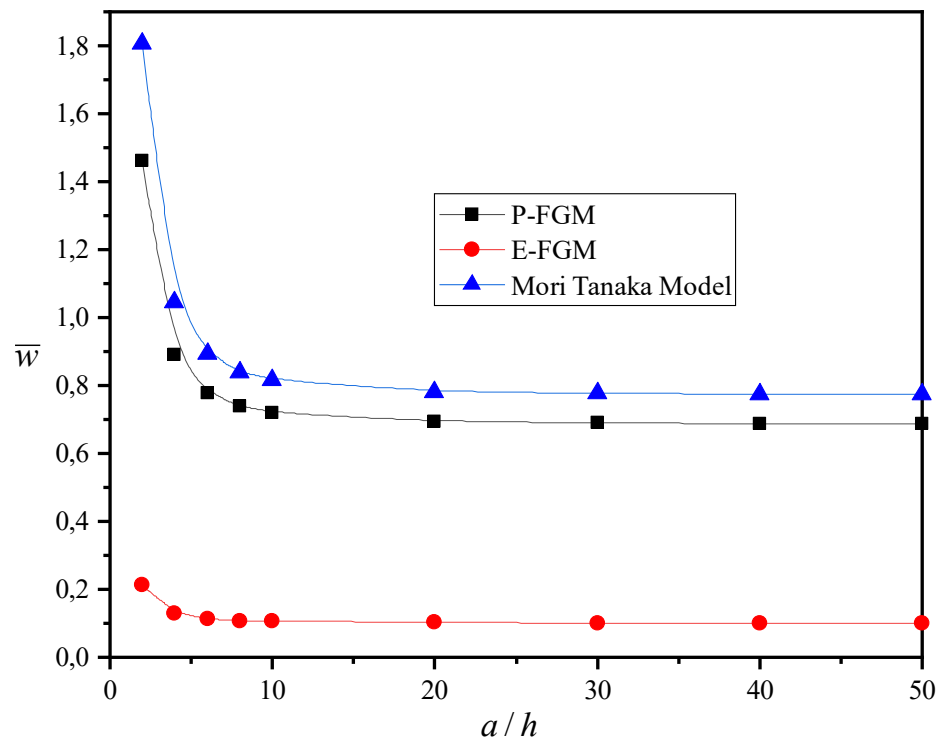


Figure 6. Effect of the side-to-thickness ratio (a/h) on the non-dimensional deflection of different FG plates.

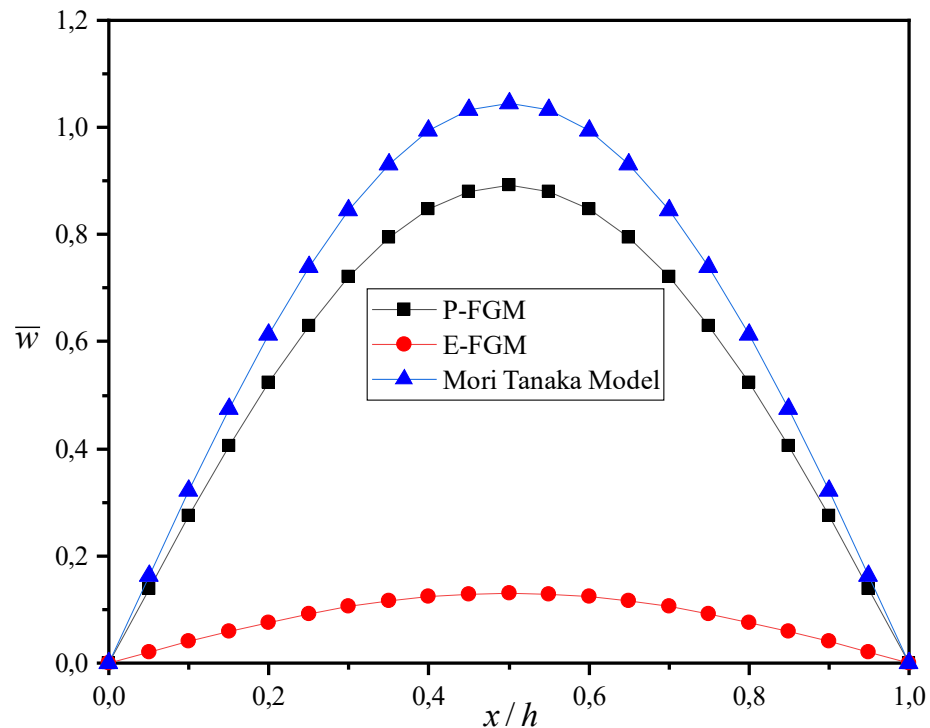


Figure 7. Comparison of the deflection of the Mori–Tanaka model and P-FGM and E-FGM plates ($a/h = 4, k = 2$).

4.2. Analysis of FG Plates on Elastic Foundation

This section aims to demonstrate the accuracy of the proposed new models in predicting the static response of FG plates resting on elastic foundation. The following relations of non-dimensional displacements, stresses and foundation parameters in the bending problem are used:

$$\begin{aligned}
 u^* &= \frac{100D_c}{q_0a^4} u\left(0, \frac{b}{2}, -\frac{h}{2}\right), v^* = \frac{100D_c}{q_0a^4} v\left(\frac{b}{2}, 0, -\frac{h}{2}\right), \\
 w^* &= \frac{100D_c}{q_0a^4} w\left(\frac{a}{2}, \frac{b}{2}\right), \sigma_x^* = -\frac{h^2}{q_0a^2} \sigma_x\left(\frac{a}{2}, \frac{b}{2}, -\frac{h}{2}\right) \\
 \sigma_y^* &= -\frac{h^2}{q_0a^2} \sigma_y\left(\frac{a}{2}, \frac{b}{2}, -\frac{h}{2}\right), \sigma_{xy}^* = \frac{h^2}{q_0a^2} \sigma_{xy}\left(0, 0, -\frac{h}{2}\right) \tag{29} \\
 K_0 &= \frac{K_w a^4}{E_0 h^3}, J_0 = \frac{K_s a^2}{\nu E_0 h^3}, E_0 = 1 \text{ GPa} \\
 \bar{K}_w &= \frac{K_w a^4}{D_c}, \bar{K}_s = \frac{K_s a^2}{D_c}, D_c = \frac{E_c h^3}{12(1-\nu^2)}
 \end{aligned}$$

In the first example, isotropic square plates on elastic foundation are analysed to verify the accuracy of the proposed theories. The dimensionless deflection of a homogeneous square plate subjected to uniform loads is presented in Table 8 for two values of the side-to-thickness ratio (a/h) and different values of the foundation parameters (\bar{K}_w, \bar{K}_s). The obtained results are compared to those given by Thai and Choi [29] using the differential quadrature method and those of Al Khateeb and Zenkour [28] based on refined shear deformation plate theory. This table proves that the computed results are in excellent agreement with those reported by the other theories of Thai and Choi [29] and Al Khateeb and Zenkour [28] for all values of side-to-thickness ratio and foundation parameters.

Table 8. Comparison of the dimensionless deflection w^* of isotropic square plate subjected to uniformly distributed load.

\bar{K}_w	\bar{K}_s	$a/h = 10$				$a/h = 200$			
		Thai et al. [24]	Al Khateeb and Zenkour [28]	Present 2D	Present Quasi-3D	Thai et al. [24]	Al Khateeb and Zenkour [28]	Present 2D	Present Quasi-3D
1	5	3.3455	3.18068	3.3452	3.3302	3.2200	3.21959	3.2200	3.2117
	10	2.7504	2.61977	2.7503	2.7452	2.6684	2.66809	2.6684	2.6628
	15	2.3331	2.2253	2.3330	2.3329	2.2763	2.27602	2.2763	2.2722
	20	2.0244	1.93304	2.0243	2.0270	1.9834	1.98317	1.9834	1.9803
3^4	5	2.8421	2.70699	2.8420	2.8358	2.7552	2.75485	2.7552	2.7491
	10	2.3983	2.28765	2.3982	2.3977	2.3390	2.33866	2.3389	2.3346
	15	2.0730	1.97963	2.0729	2.0754	2.0306	2.03037	2.0306	2.0274
	20	1.8244	1.74394	1.8244	1.8286	1.7932	1.79298	1.7932	1.7907
5^4	5	1.3785	1.32344	1.3784	1.3854	1.3688	1.36864	1.3688	1.3674
	10	1.2615	1.21169	1.2614	1.2684	1.2543	1.25412	1.2542	1.2531
	15	1.1627	1.11725	1.1627	1.1694	1.1572	1.15711	1.1572	1.1562
	20	1.0782	1.03638	1.0782	1.0847	1.0740	1.07389	1.0740	1.0732

The next example is implemented for Al/Al₂O₃ moderately thick rectangular plates on elastic foundation. Table 9 presents a comparison of non-dimensional displacements and stresses of FG plate for various exponent values (k) and foundation parameters (K_0, J_0), derived from the present theory, the sinusoidal shear deformation theory of Zenkour [20], and the 2D zeroth-order shear deformation theory of Thai and Choi [29]. It is clear that the present results are found to be closer with other theories for the different parameters. It should be noted that the present theory is not only efficient but more accurate in predicting the bending behaviour of FG plates resting on elastic foundation. The table exhibits that axial displacements, deflection, and stresses decrease with the increase in foundation parameters. In addition, it is apparent that the computed values from the present quasi-3D theory which takes into account the thickness stretching effect are smaller than those calculated from 2D theory.

Table 9. Comparisons of non-dimensional displacements and stresses of simply supported FG rectangular plate (Al/Al₂O₃) resting on elastic foundation under uniform loads ($b = 3a, a/h = 10$).

k	K_0	J_0	Method	u^*	v^*	w^*	σ_x^*	σ_y^*	σ_{xy}^*
0	0	0	Zenkour [20]	0.1972	0.1022	1.2583	0.7162	0.2448	0.2893
			Thai and Choi [29]	0.1971	0.1022	1.2583	0.7160	0.2447	0.2890
			Present 2D	0.1972	0.1021	1.2582	0.7159	0.2442	0.2869
			Present Quasi-3D	0.1953	0.1009	1.2503	0.8755	0.4074	0.2823
	100	0	Zenkour [20]	0.1922	0.1003	1.2259	0.6970	0.2376	0.2843
			Thai and Choi [29]	0.1922	0.1003	1.2260	0.6969	0.2375	0.2840
			Present 2D	0.1922	0.1002	1.2259	0.6967	0.2370	0.2819
			Present Quasi-3D	0.1905	0.0991	1.2186	0.8523	0.3959	0.2774

Table 9. *Cont.*

k	K_0	J_0	Method	u^*	v^*	w^*	σ_x^*	σ_y^*	σ_{xy}^*
0.5	0	100	Zenkour [20]	0.1830	0.0967	1.1662	0.6619	0.2245	0.2746
			Thai and Choi [29]	0.1830	0.0967	1.1662	0.6618	0.2245	0.2744
			Present 2D	0.1830	0.0966	1.1661	0.6616	0.2239	0.2723
			Present Quasi-3D	0.1815	0.0955	1.1599	0.8097	0.3749	0.2681
	100	100	Zenkour [20]	0.1787	0.0951	1.1382	0.6453	0.2184	0.2702
			Thai and Choi [29]	0.1787	0.0951	1.1382	0.6452	0.2183	0.2700
			Present 2D	0.1787	0.0950	1.1381	0.6451	0.2178	0.2679
			Present Quasi-3D	0.1772	0.0939	1.1323	0.7895	0.3650	0.2638
	0	0	Zenkour [20]	0.3492	0.1810	1.9344	0.2337	0.0799	0.0941
			Thai and Choi [29]	0.3491	0.1809	1.9345	0.2337	0.0799	0.0941
			Present 2D	0.3492	0.1807	1.9343	0.2336	0.0797	0.0934
			Present Quasi-3D	0.3346	0.1729	1.8995	0.2763	0.1286	0.0891
	100	0	Zenkour [20]	0.3358	0.1759	1.8590	0.2242	0.0763	0.0916
			Thai and Choi [29]	0.3358	0.1758	1.8590	0.2242	0.0763	0.0916
			Present 2D	0.3358	0.1756	1.8589	0.2242	0.0761	0.0910
			Present Quasi-3D	0.3221	0.1681	1.8271	0.2653	0.1231	0.0867
	0	100	Zenkour [20]	0.3120	0.1665	1.7248	0.2075	0.0701	0.0871
			Thai and Choi [29]	0.3119	0.1665	1.7248	0.2075	0.0701	0.0870
			Present 2D	0.3120	0.1663	1.7247	0.2074	0.0699	0.0864
			Present Quasi-3D	0.2997	0.1593	1.6980	0.2458	0.1136	0.0824
100	100	Zenkour [20]	0.3013	0.1623	1.6640	0.1999	0.0673	0.0850	
		Thai and Choi [29]	0.3012	0.1623	1.6640	0.1999	0.0673	0.0850	
		Present 2D	0.3013	0.1621	1.6639	0.1998	0.0671	0.0843	
		Present Quasi-3D	0.2896	0.1554	1.6394	0.2369	0.1092	0.0805	
0	0	Zenkour [20]	0.4855	0.2515	2.5133	0.3250	0.1111	0.1307	
		Thai and Choi [29]	0.4854	0.2515	2.5134	0.3250	0.1111	0.1306	
		Present 2D	0.4854	0.2512	2.5132	0.3249	0.1108	0.1298	
		Present Quasi-3D	0.4544	0.2347	2.4287	0.3752	0.1746	0.1209	
100	0	Zenkour [20]	0.4617	0.2424	2.3874	0.3081	0.1047	0.1263	
		Thai and Choi [29]	0.4616	0.2424	2.3875	0.3080	0.1047	0.1262	
		Present 2D	0.4616	0.2421	2.3873	0.3080	0.1045	0.1254	
		Present Quasi-3D	0.4329	0.2265	2.3115	0.3563	0.1652	0.1170	
0	100	Zenkour [20]	0.4204	0.2262	2.1702	0.2791	0.0940	0.1183	
		Thai and Choi [29]	0.4203	0.2261	2.1703	0.2791	0.0940	0.1182	
		Present 2D	0.4204	0.2258	2.1701	0.2790	0.0938	0.1174	
		Present Quasi-3D	0.3955	0.2118	2.1083	0.3238	0.1493	0.1097	
100	100	Zenkour [20]	0.4023	0.2191	2.0746	0.2663	0.0893	0.1148	
		Thai and Choi [29]	0.4022	0.2190	2.0746	0.2663	0.0893	0.1148	
		Present 2D	0.4023	0.2188	2.0745	0.2662	0.0890	0.1139	
		Present Quasi-3D	0.3790	0.2054	2.0184	0.3093	0.1422	0.1066	

Table 9. Cont.

k	K_0	J_0	Method	u^*	v^*	w^*	σ_x^*	σ_y^*	σ_{xy}^*
2	0	0	Zenkour [20]	0.6565	0.3401	3.2267	0.4396	0.1502	0.1766
			Thai and Choi [29]	0.6564	0.3400	3.2266	0.4395	0.1502	0.1766
			Present 2D	0.6565	0.3397	3.2266	0.4394	0.1499	0.1755
			Present Quasi-3D	0.6025	0.3113	3.0706	0.4975	0.2315	0.1604
	100	0	Zenkour [20]	0.6157	0.3245	3.0219	0.4106	0.1394	0.1690
			Thai and Choi [29]	0.6156	0.3244	3.0218	0.4105	0.1394	0.1690
			Present 2D	0.6157	0.3241	3.0218	0.4104	0.1390	0.1679
			Present Quasi-3D	0.5669	0.2977	2.8854	0.4661	0.2160	0.1538
	0	100	Zenkour [20]	0.5476	0.2975	2.6814	0.3628	0.1217	0.1557
			Thai and Choi [29]	0.5475	0.2974	2.6814	0.3628	0.1217	0.1557
			Present 2D	0.5475	0.2971	2.6813	0.3627	0.1214	0.1546
			Present Quasi-3D	0.5069	0.2740	2.5748	0.4141	0.1904	0.1421
100	100	Zenkour [20]	0.5187	0.2861	2.5364	0.3423	0.1142	0.1502	
		Thai and Choi [29]	0.5186	0.2860	2.5364	0.3423	0.1142	0.1501	
		Present 2D	0.5187	0.2856	2.5363	0.3422	0.1138	0.1490	
		Present Quasi-3D	0.4813	0.2639	2.4415	0.3916	0.1794	0.1372	
5	0	0	Zenkour [20]	0.7805	0.4045	3.8517	0.5224	0.1785	0.2104
			Thai and Choi [29]	0.7802	0.4043	3.8506	0.5223	0.1785	0.2103
			Present 2D	0.7804	0.4040	3.8516	0.5222	0.1781	0.2089
			Present Quasi-3D	0.7198	0.3721	3.6893	0.5941	0.2765	0.1919
	100	0	Zenkour [20]	0.7232	0.3825	3.5629	0.4816	0.1633	0.1997
			Thai and Choi [29]	0.7230	0.3824	3.5620	0.4816	0.1633	0.1996
			Present 2D	0.7231	0.3820	3.5628	0.4816	0.1629	0.1982
			Present Quasi-3D	0.6693	0.3528	3.4247	0.5496	0.2544	0.1825
	0	100	Zenkour [20]	0.6305	0.3456	3.0979	0.4168	0.1394	0.1815
			Thai and Choi [29]	0.6304	0.3455	3.0972	0.4168	0.1394	0.1814
			Present 2D	0.6304	0.3451	3.0978	0.4166	0.1390	0.1800
			Present Quasi-3D	0.5868	0.3199	2.9948	0.4781	0.2194	0.1663
100	100	Zenkour [20]	0.5923	0.3304	2.9052	0.3897	0.1294	0.1741	
		Thai and Choi [29]	0.5922	0.3303	2.9046	0.3897	0.1294	0.1740	
		Present 2D	0.5922	0.3298	2.9050	0.3895	0.1290	0.1726	
		Present Quasi-3D	0.5524	0.3063	2.8153	0.4481	0.2047	0.1597	

To check the effect of Winkler’s and Pasternak’s foundation parameters (\bar{K}_w, \bar{K}_s) on the bending behaviour of FG plates subjected to sinusoidal loads based on the proposed 2D and quasi-3D theories, Figure 8 depicts the variation in non-dimensional deflection \bar{w} of Al/Al₂O₃ FG square plates versus Winkler (\bar{K}_w) and Pasternak (\bar{K}_s) parameters. As can be seen from this figure, the dimensionless deflection diminishes when the foundation parameters increase. Compared to the Winkler parameter (\bar{K}_w), the Pasternak foundation parameter (\bar{K}_s) has a more significant effect on decreasing the dimensionless deflection. Additionally, the deflection computed by present quasi-3D theory is lower than that obtained from 2D theory, which means the thickness-stretching effect is more significant when the thickness of the plate is higher, but it is negligible with reducing the thickness of the

plate. This indicates that the stretching effect is pronounced and must be taken into account in the modelling of thick plate.

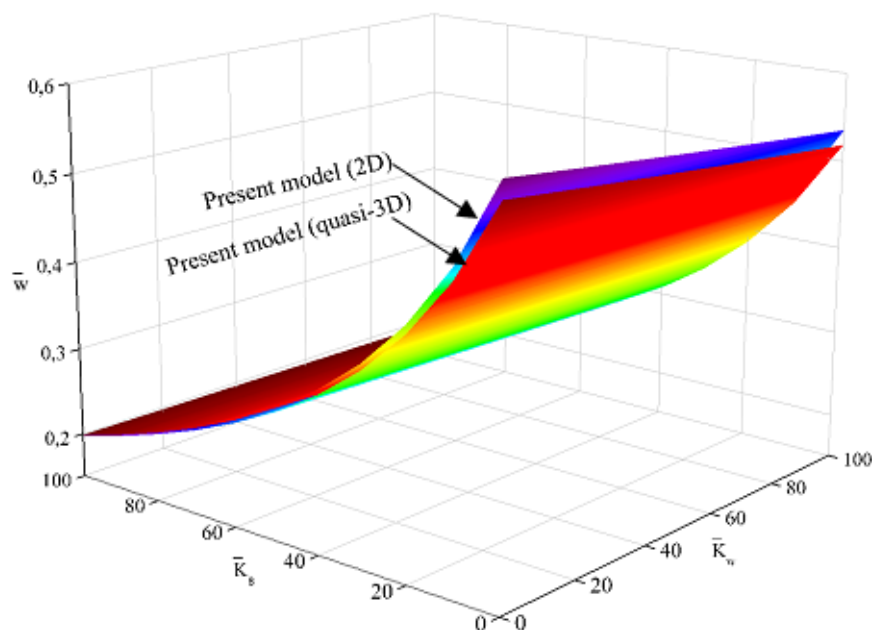


Figure 8. Effect of foundation parameters (\bar{K}_w, \bar{K}_s) on the non-dimensional deflection \bar{w} of FG square plates under sinusoidal load ($k=1, a/h=10$).

5. Conclusions

The aim of this work is to develop a mathematical approach in order to study the mechanical behaviour of functionally graded plates on elastic foundation by applying the 2D and quasi-3D shear strain theories proposed by Zaoui et al. (2019) regarding free vibration analysis. The theory, in which only five unknowns are used, takes into account a parabolic distribution of the transverse shear stress using a new shear shape function which satisfies the boundary conditions with no tension or compression on the bottom and top surfaces of the plate. Moreover, the shear correction factor has not been included. The principle of virtual work was applied to determine the equilibrium equations. The analytical solutions of simply supported plates are obtained using the double Fourier series and are compared to previously published solutions in order to demonstrate the accuracy of the proposed theory. The effects of a large number of parameters, such as the transverse normal strain, the form ratio of the plate, the length/thickness ratio, the volume fraction distributions, the various mixing laws, and the boundary conditions on the deflection, axial displacements and the various stresses are examined in detail. From the results analysed above, the following main points can be drawn:

- Through all the comparative investigations, it can be seen that the proposed theory proves good agreement with the results of other 2D and quasi-3D HSDTs.
- The proposed quasi-3D HSDT contains five unknowns but provides results comparable to those generated by other published quasi-3D theories with greater numbers of unknowns (e.g., quasi-3D theories of Neves et al. [22,23] with nine unknowns and Akavci and Tanrikulu [31] with six unknowns).
- The power law index has the effect of increasing deflections of plate. The influence of the value of material index more than 5 is negligible.
- The small difference between the present 2D and quasi-3D shear deformation results is due to neglecting the thickness stretching effect.
- Results demonstrate that the plate becomes stiffer when the effects of normal deformations are considered, consequently leading to a decrease in deflection and an increase in stresses.

- The thickness stretching effect is more pronounced for thick plates and it needs to be taken into account in the modelling.
- The decreasing effect of foundation parameters on the deflection leads to an increase in the FG plate stiffness.

Consequently, the present method yields more accurate results for plate bending problems, as they are closer when compared to those reported in other literatures using numerical methods. Finally, it can be concluded that the formulation developed herein can serve as a reference for future research and could be extended to the analysis of classical and thermal buckling of FG plates by introducing various combined boundary conditions. Additionally, the present method can be combined with the nonlocal continuum mechanics to model the nano and micro material mechanical behaviours.

Author Contributions: Methodology and supervision, D.O.; project administration, writing—review and editing, B.A.; software and writing—original draft preparation, F.Z.Z.; visualization, M.B.; validation, J.A.V.O. and A.A.A.A.-N.; investigation, E.R.L. and M.T. All authors have read and agreed to the published version of the manuscript.

Funding: This research was funded by Deanship of Scientific Research at the University of Hail, Saudi Arabia, under the project number RG-20 098.

Data Availability Statement: Not applicable.

Acknowledgments: The authors would like to express their deepest gratitude to the Deanship of Scientific Research and to the College of Engineering at the University of Hail, for providing necessary support for conducting this research, through the project number RG-20 098.

Conflicts of Interest: The authors declare no conflict of interest.

Nomenclature

Parameters	Description	Units	Parameters	Description	Units
a	Length	m	p	Power law index	/
b	Width	m	σ_{ij}	Stress tensor	$N m^{-2}$
h	Thickness	m	ϵ_{ij}	Strain tensor	
E	Young’s modulus	GPa	Q_{ij}	Engineering constants	GPa
ν	Poisson ratio	/	u, v, w	Displacements in x, y, z axis.	m
ρ	Mass Density	Kg/m^3	q	Mechanical load	N
P	Material property	/	$f(z)$	Shape function	/
V	Volume fraction	/	m, n	modes	/

References

1. Jha, D.K.; Kant, T.; Singh, R.K. Higher Order Shear and Normal Deformation Theory for Natural Frequency of Functionally Graded Rectangular Plates. *Nucl. Eng. Des.* **2012**, *250*, 8–13. [CrossRef]
2. Hebali, H.; Tounsi, A.; Houari, M.S.A.; Bessaim, A.; Bedia, E.A.A. New Quasi-3D Hyperbolic Shear Deformation Theory for the Static and Free Vibration Analysis of Functionally Graded Plates. *J. Eng. Mech.* **2014**, *140*, 374–383. [CrossRef]
3. Nguyen, T.-K. A Higher-Order Hyperbolic Shear Deformation Plate Model for Analysis of Functionally Graded Materials. *Int. J. Mech. Mater. Des.* **2015**, *11*, 203–219. [CrossRef]
4. Abdulrazzaq, M.A.; Fenjan, R.M.; Ahmed, R.A.; Faleh, N.M. Thermal Buckling of Nonlocal Clamped Exponentially Graded Plate According to a Secant Function Based Refined Theory. *Steel Compos. Struct.* **2020**, *35*, 147–157.
5. Alijani, F.; Amabili, M. Effect of Thickness Deformation on Large-Amplitude Vibrations of Functionally Graded Rectangular Plates. *Compos. Struct.* **2014**, *113*, 89–107. [CrossRef]
6. Arefi, M.; Allam, M.N.M. Nonlinear Responses of an Arbitrary FGP Circular Plate Resting on the Winkler-Pasternak Foundation. *Smart Struct. Syst.* **2015**, *16*, 81–100. [CrossRef]
7. Amir, S.; Arshid, E.; Rasti-Alhosseini, S.M.A.; Loghman, A. Quasi-3D Tangential Shear Deformation Theory for Size-Dependent Free Vibration Analysis of Three-Layered FG Porous Micro Rectangular Plate Integrated by Nano-Composite Faces in Hygrothermal Environment. *J. Therm. Stresses* **2020**, *43*, 133–156. [CrossRef]
8. Azadi, M. Free and Forced Vibration Analysis of FG Beam Considering Temperature Dependency of Material Properties. *J. Mech. Sci. Technol.* **2011**, *25*, 69–80. [CrossRef]

9. Zaoui, F.Z.; Ouinas, D.; Tounsi, A.; Viña Olay, J.A.; Achour, B.; Touahmia, M. Fundamental Frequency Analysis of Functionally Graded Plates with Temperature-Dependent Properties Based on Improved Exponential-Trigonometric Two-Dimensional Higher Shear Deformation Theory. *Arch. Appl. Mech.* **2021**, *91*, 859–881. [[CrossRef](#)]
10. Hosseini-Hashemi, S.; Rokni Damavandi Taher, H.; Akhavan, H.; Omid, M. Free Vibration of Functionally Graded Rectangular Plates Using First-Order Shear Deformation Plate Theory. *Appl. Math. Model.* **2010**, *34*, 1276–1291. [[CrossRef](#)]
11. Golmakani, M.E.; Alamatian, J. Large Deflection Analysis of Shear Deformable Radially Functionally Graded Sector Plates on Two-Parameter Elastic Foundations. *Eur. J. Mech.-A/Solids* **2013**, *42*, 251–265. [[CrossRef](#)]
12. Duc, N.D.; Quan, T.Q. Nonlinear Dynamic Analysis of Imperfect Functionally Graded Material Double Curved Thin Shallow Shells with Temperature-Dependent Properties on Elastic Foundation. *J. Vib. Control* **2015**, *21*, 1340–1362. [[CrossRef](#)]
13. Khalili, A.; Vosoughi, A.R. An Approach for the Pasternak Elastic Foundation Parameters Estimation of Beams Using Simulated Frequencies. *Inverse Probl. Sci. Eng.* **2018**, *26*, 1079–1093. [[CrossRef](#)]
14. Meksi, A.; Benyoucef, S.; Houari, M.S.A.; Tounsi, A. A Simple Shear Deformation Theory Based on Neutral Surface Position for Functionally Graded Plates Resting on Pasternak Elastic Foundations. *Struct. Eng. Mech. Int. J.* **2015**, *53*, 1215–1240. [[CrossRef](#)]
15. Shahbaztabar, A.; Ranji, A.R. Effects of In-Plane Loads on Free Vibration of Symmetrically Cross-Ply Laminated Plates Resting on Pasternak Foundation and Coupled with Fluid. *Ocean Eng.* **2016**, *115*, 196–209. [[CrossRef](#)]
16. Radaković, A.; Čukanović, D.; Bogdanović, G.; Blagojević, M.; Stojanović, B.; Dragović, D.; Manić, N. Thermal Buckling and Free Vibration Analysis of Functionally Graded Plate Resting on an Elastic Foundation According to High Order Shear Deformation Theory Based on New Shape Function. *Appl. Sci.* **2020**, *10*, 4190. [[CrossRef](#)]
17. Zenkour, A.M.; El-Shahrany, H.D. Hygrothermal Forced Vibration of a Viscoelastic Laminated Plate with Magnetostrictive Actuators Resting on Viscoelastic Foundations. *Int. J. Mech. Mater. Des.* **2021**, *17*, 301–320. [[CrossRef](#)]
18. Zaoui, F.Z.; Ouinas, D.; Achour, B.; Tounsi, A.; Latifee, E.R.; Al-Naghi, A.A.A. A Hyperbolic Shear Deformation Theory for Natural Frequencies Study of Functionally Graded Plates on Elastic Supports. *J. Compos. Sci.* **2022**, *6*, 285. [[CrossRef](#)]
19. Zenkour, A.M. Benchmark Trigonometric and 3-D Elasticity Solutions for an Exponentially Graded Thick Rectangular Plate. *Arch. Appl. Mech.* **2007**, *77*, 197–214. [[CrossRef](#)]
20. Zenkour, A.M. The Refined Sinusoidal Theory for FGM Plates on Elastic Foundations. *Int. J. Mech. Sci.* **2009**, *51*, 869–880. [[CrossRef](#)]
21. Carrera, E.; Brischetto, S.; Cinefra, M.; Soave, M. Effects of Thickness Stretching in Functionally Graded Plates and Shells. *Compos. Part B Eng.* **2011**, *42*, 123–133. [[CrossRef](#)]
22. Neves, A.M.A.; Ferreira, A.J.M.; Carrera, E.; Roque, C.M.C.; Cinefra, M.; Jorge, R.M.N.; Soares, C.M.M. A Quasi-3D Sinusoidal Shear Deformation Theory for the Static and Free Vibration Analysis of Functionally Graded Plates. *Compos. Part B Eng.* **2012**, *43*, 711–725. [[CrossRef](#)]
23. Neves, A.M.A.; Ferreira, A.J.M.; Carrera, E.; Cinefra, M.; Roque, C.M.C.; Jorge, R.M.N.; Soares, C.M.M. A Quasi-3D Hyperbolic Shear Deformation Theory for the Static and Free Vibration Analysis of Functionally Graded Plates. *Compos. Struct.* **2012**, *94*, 1814–1825. [[CrossRef](#)]
24. Thai, H.-T.; Park, M.; Choi, D.-H. A Simple Refined Theory for Bending, Buckling, and Vibration of Thick Plates Resting on Elastic Foundation. *Int. J. Mech. Sci.* **2013**, *73*, 40–52. [[CrossRef](#)]
25. Ouinas, D.; Achour, B. Buckling Analysis of Laminated Composite Plates $[(\theta/-\theta)]$ Containing an Elliptical Notch. *Compos. Part B Eng.* **2013**, *55*, 575–579. [[CrossRef](#)]
26. Mantari, J.L.; Guedes Soares, C. A Novel Higher-Order Shear Deformation Theory with Stretching Effect for Functionally Graded Plates. *Compos. Part B Eng.* **2013**, *45*, 268–281. [[CrossRef](#)]
27. Zhang, H.; Jiang, J.; Zhang, Z. Three-Dimensional Elasticity Solutions for Bending of Generally Supported Thick Functionally Graded Plates. *Appl. Math. Mech.-Engl. Ed.* **2014**, *35*, 1467–1478. [[CrossRef](#)]
28. Al Khateeb, S.A.; Zenkour, A.M. A Refined Four-Unknown Plate Theory for Advanced Plates Resting on Elastic Foundations in Hygrothermal Environment. *Compos. Struct.* **2014**, *111*, 240–248. [[CrossRef](#)]
29. Thai, H.-T.; Choi, D.-H. Zeroth-Order Shear Deformation Theory for Functionally Graded Plates Resting on Elastic Foundation. *Int. J. Mech. Sci.* **2014**, *78*, 35–43. [[CrossRef](#)]
30. Lee, W.-H.; Han, S.-C.; Park, W.-T. A Refined Higher Order Shear and Normal Deformation Theory for E-, P-, and S-FGM Plates on Pasternak Elastic Foundation. *Compos. Struct.* **2015**, *122*, 330–342. [[CrossRef](#)]
31. Akavci, S.S.; Tanrikulu, A.H. Static and Free Vibration Analysis of Functionally Graded Plates Based on a New Quasi-3D and 2D Shear Deformation Theories. *Compos. Part B Eng.* **2015**, *83*, 203–215. [[CrossRef](#)]
32. Mantari, J.L.; Granados, E.V. An Original FSDT to Study Advanced Composites on Elastic Foundation. *Thin-Walled Struct.* **2016**, *107*, 80–89. [[CrossRef](#)]
33. Houari, M.S.A.; Tounsi, A.; Bessaim, A.; Mahmoud, S.R. A New Simple Three-Unknown Sinusoidal Shear Deformation Theory for Functionally Graded Plates. *Steel Compos. Struct.* **2016**, *22*, 257–276. [[CrossRef](#)]
34. Aldousari, S.M. Bending Analysis of Different Material Distributions of Functionally Graded Beam. *Appl. Phys. A* **2017**, *123*, 296. [[CrossRef](#)]
35. Meftah, A.; Bakora, A.; Zaoui, F.Z.; Tounsi, A.; Bedia, E.A.A. A Non-Polynomial Four Variable Refined Plate Theory for Free Vibration of Functionally Graded Thick Rectangular Plates on Elastic Foundation. *Steel Compos. Struct.* **2017**, *23*, 317–330. [[CrossRef](#)]

36. Zaoui, F.Z.; Tounsi, A.; Ouinas, D. Free Vibration of Functionally Graded Plates Resting on Elastic Foundations Based on Quasi-3D Hybrid-Type Higher Order Shear Deformation Theory. *Smart Struct. Syst.* **2017**, *20*, 509–524.
37. Guerroudj, H.Z.; Yeghnem, R.; Kaci, A.; Zaoui, F.Z.; Benyoucef, S.; Tounsi, A. Eigenfrequencies of Advanced Composite Plates Using an Efficient Hybrid Quasi-3D Shear Deformation Theory. *Smart Struct. Syst.* **2018**, *22*, 121–132.
38. Amar, L.H.H.; Kaci, A.; Yeghnem, R.; Tounsi, A. A New Four-Unknown Refined Theory Based on Modified Couple Stress Theory for Size-Dependent Bending and Vibration Analysis of Functionally Graded Micro-Plate. *Steel Compos. Struct.* **2018**, *26*, 89–102. [[CrossRef](#)]
39. Younsi, A.; Tounsi, A.; Zaoui, F.Z.; Bousahla, A.A.; Mahmoud, S.R. Novel Quasi-3D and 2D Shear Deformation Theories for Bending and Free Vibration Analysis of FGM Plates. *Geomech. Eng.* **2018**, *14*, 519–532.
40. Belkhouja, Y.; Ouinas, D.; Zaoui, F.Z.; Fekirini, H. An Exponential-Trigonometric Higher Order Shear Deformation Theory (HSDT) for Bending, Free Vibration, and Buckling Analysis of Functionally Graded Materials (FGMs) Plates. *Adv. Compos. Lett.* **2020**, *29*, 096369351987573. [[CrossRef](#)]
41. Wang, Y.; Zeng, R.; Safarpour, M. Vibration Analysis of FG-GPLRC Annular Plate in a Thermal Environment. *Mech. Based Des. Struct. Mach.* **2022**, *50*, 352–370. [[CrossRef](#)]
42. Shah, N.A.; Wakif, A.; El-Zahar, E.R.; Ahmad, S.; Yook, S.-J. Numerical Simulation of a Thermally Enhanced EMHD Flow of a Heterogeneous Micropolar Mixture Comprising (60%)-Ethylene Glycol (EG), (40%)-Water (W), and Copper Oxide Nanomaterials (CuO). *Case Stud. Therm. Eng.* **2022**, *35*, 102046. [[CrossRef](#)]
43. Sajjan, K.; Shah, N.A.; Ahammad, N.A.; Raju, C.S.K.; Kumar, M.D.; Weera, W.; Sajjan, K.; Shah, N.A.; Ahammad, N.A.; Raju, C.S.K.; et al. Nonlinear Boussinesq and Rosseland Approximations on 3D Flow in an Interruption of Ternary Nanoparticles with Various Shapes of Densities and Conductivity Properties. *AIMS Math.* **2022**, *7*, 18416–18449. [[CrossRef](#)]
44. Raza, Q.; Qureshi, M.Z.A.; Khan, B.A.; Kadhim Hussein, A.; Ali, B.; Shah, N.A.; Chung, J.D. Insight into Dynamic of Mono and Hybrid Nanofluids Subject to Binary Chemical Reaction, Activation Energy, and Magnetic Field through the Porous Surfaces. *Mathematics* **2022**, *10*, 3013. [[CrossRef](#)]
45. Sabu, A.S.; Wakif, A.; Areekara, S.; Mathew, A.; Shah, N.A. Significance of Nanoparticles' Shape and Thermo-Hydrodynamic Slip Constraints on MHD Alumina-Water Nanoliquid Flows over a Rotating Heated Disk: The Passive Control Approach. *Int. Commun. Heat Mass Transf.* **2021**, *129*, 105711. [[CrossRef](#)]
46. Qureshi, M.Z.A.; Faisal, M.; Raza, Q.; Ali, B.; Botmart, T.; Shah, N.A.; Qureshi, M.Z.A.; Faisal, M.; Raza, Q.; Ali, B.; et al. Morphological Nanolayer Impact on Hybrid Nanofluids Flow Due to Dispersion of Polymer/CNT Matrix Nanocomposite Material. *AIMS Math.* **2023**, *8*, 633–656. [[CrossRef](#)]
47. Mahsud, Y.; Shah, N.A.; Vieru, D. Influence of Time-Fractional Derivatives on the Boundary Layer Flow of Maxwell Fluids. *Chin. J. Phys.* **2017**, *55*, 1340–1351. [[CrossRef](#)]
48. Elnaqeeb, T.; Shah, N.A.; Mirza, I.A. Natural Convection Flows of Carbon Nanotubes Nanofluids with Prabhakar-like Thermal Transport. *Math. Methods Appl. Sci.* **2020**. [[CrossRef](#)]
49. Vieru, D.; Fetecau, C.; Shah, N.A.; Yook, S.-J. Unsteady Natural Convection Flow Due to Fractional Thermal Transport and Symmetric Heat Source/Sink. *Alex. Eng. J.* **2022**, *in press*. [[CrossRef](#)]
50. Saffari, P.R.; Fakhraie, M.; Roudbari, M.A. Nonlinear Vibration of Fluid Conveying Cantilever Nanotube Resting on Visco-Pasternak Foundation Using Non-Local Strain Gradient Theory. *Micro Nano Lett.* **2020**, *15*, 181–186. [[CrossRef](#)]
51. Alazwari, M.A.; Zenkour, A.M. A Quasi-3D Refined Theory for the Vibration of Functionally Graded Plates Resting on Visco-Winkler-Pasternak Foundations. *Mathematics* **2022**, *10*, 716. [[CrossRef](#)]
52. Zaoui, F.Z.; Ouinas, D.; Tounsi, A. New 2D and Quasi-3D Shear Deformation Theories for Free Vibration of Functionally Graded Plates on Elastic Foundations. *Compos. Part B Eng.* **2019**, *159*, 231–247. [[CrossRef](#)]
53. Zaoui, F.Z.; Hanifi, H.A.L.; Younsi, A.; Meradjah, M.; Tounsi, A.; Ouinas, D. Free Vibration Analysis of Functionally Graded Beams Using a Higher-Order Shear Deformation Theory. *Math. Model. Eng. Probl.* **2017**, *4*, 7–12. [[CrossRef](#)]
54. Meradjah, M.; Bouakkaz, K.; Zaoui, F.Z.; Tounsi, A. A Refined Quasi-3D Hybrid-Type Higher Order Shear Deformation Theory for Bending and Free Vibration Analysis of Advanced Composites Beams. *Wind. Struct.* **2018**, *27*, 269–282.
55. Zaoui, F.Z.; Tounsi, A.; Ouinas, D.; Viña Olay, J.A. A Refined HSDT for Bending and Dynamic Analysis of FGM Plates. *Struct. Eng. Mech. Int'l J.* **2020**, *74*, 105–119.
56. Zenkour, A.M.; Hafed, Z.S.; Radwan, A.F. Bending Analysis of Functionally Graded Nanoscale Plates by Using Nonlocal Mixed Variational Formula. *Mathematics* **2020**, *8*, 1162. [[CrossRef](#)]
57. Rachid, A.; Ouinas, D.; Lousdad, A.; Zaoui, F.Z.; Achour, B.; Gasmi, H.; Butt, T.A.; Tounsi, A. Mechanical Behavior and Free Vibration Analysis of FG Doubly Curved Shells on Elastic Foundation via a New Modified Displacements Field Model of 2D and Quasi-3D HSDTs. *Thin-Walled Struct.* **2022**, *172*, 108783. [[CrossRef](#)]
58. Vaghefi, R.; Baradaran, G.H.; Koohkan, H. Three-Dimensional Static Analysis of Thick Functionally Graded Plates by Using Meshless Local Petrov–Galerkin (MLPG) Method. *Eng. Anal. Bound. Elem.* **2010**, *34*, 564–573. [[CrossRef](#)]